LOW TEMPERATURE OPERATION OF APD
FOR QUANTUM CRYPTOGRAPHIC APPLICATIONS

A THESIS SUBMITTED TO

THE GRADUATE SCHOOL OF NATURAL AND APPLIED SCIENCES

OF

MIDDLE EAST TECHNICAL UNIVERSITY

BY

ZÜHAL KALE

IN PARTIAL FULFILLMENT OF THE REQUIREMENTS

FOR

THE DEGREE OF MASTER OF SCIENCE

IN

ELECTRICAL AND ELECTRONICS ENGINEERING

APRIL 2005

Approval of the Graduate School of Natural Sciences

Prof. Dr. Canan ÖZGEN
Director

I certify that this thesis satisfies all the requirements as a thesis for the degree of Master of Science.

Prof. Dr. İsmet ERKMEN
Chair of Electrical and Electronics
Engineering Department

This is to certify that we have read this thesis and that in our opinion it is fully adequate, in scope and quality, as a thesis for the degree of Master of Science.

Co-Supervisor

Prof. Dr. Rüyal ERGÜL
Supervisor

Examining Committee Members

Prof. Dr. Murat AŞKAR	(EE Eng.)	
Prof. Dr. Rüyal ERGÜL	(EE Eng.)	
Assoc. Prof. Dr. Melek YÜCEL	(EE Eng.)	
Assoc. Prof. Dr. Sencer KOÇ	(EE Eng.)	
Assoc. Prof. Dr. Yusuf İPEKOĞLU	(Physics Department)	

I hereby declare that all information in this document has been obtained and presented in accordance with academic rules and ethical conduct. I also declare that, as required by these rules and conduct, I have fully cited and referenced all material and results that are not original to this work.

Name, Last name : Zuhal KALE

Signature :

ABSTRACT

LOW TEMPERATURE OPERATION OF APD

FOR QUANTUM CRYPTOGRAPHIC APPLICATIONS

KALE, Zuhal
M. D., Department of Electrical and Electronics Engineering
Supervisor : Prof. Dr. Rüyal ERGÜL
Co-Supervisor:

April 2005, 59 pages

This thesis explains low temperature operation of an InGaAs Avalanche Photo Diode (APD) cooled using thermoelectric coolers in order to utilize in the quantum cryptographic applications. A theoretical background for the equipment used in the experiment was provided. Circuitry and mechanics used for the low temperature operation were designed. Performance measures for APD were explained and experiment results were presented.

Keywords: Low Temperature, APD, Quantum Cryptography

ÖZ

KUANTUM KRİPTOLOJİ UYGULAMALARI İÇİN BİR APD-NİN

DÜŞÜK SICAKLIKTA ÇALIŞTIRILMASI

KALE, Zuhal
Y. Lisans, Elektrik ve Elektronik Mühendisliği Bölümü
Tez Yöneticisi : Prof. Dr. Rüyal ERGÜL
Ortak Tez Yôneticisi:

Nisan 2005, 59 sayfa

Bu tez kuantum kriptoloji uygulamalarında faydalanmak amacıyla termoelektrik soğutucular kullanarak soğutulan InGaAs Çığ Foto Diyotun (ÇFD) düşük sıcaklıkta çalışmasını açıklamaktadır. ÇFD deneyinde kullanılacak temel teçhizat hakkında teorik bir altyapı sağlandı. Düşük sıcaklıkta çalışma için kullanılacak devre ve mekanik tasarlandı. ÇFD performans parametreleri açıklandı ve deney sonuçları sunuldu.

Anahtar Kelimeler: Düşük Sıcaklık, ÇFD, Kuantum Kriptoloji

To My Family

ACKNOWLEDGMENTS

The author wishes to express her deepest gratitude to her supervisor, Prof. Dr. Rüyal ERGÜL, for his guidance, advice, criticism and encouragement and insight throughout the research and experiment process.

Oktay KOÇ has been helpful in problems concerning mechanics and practical matters. His assistance is gratefully acknowledged.

TABLE of CONTENTS

LIST OF FIGURES

FIGURES

CHAPTER 1

INTRODUCTION

Cryptography has been studied for many years and there is a continuous process of generating secure algorithms and a constant afford to analyze and show that secure algorithms are indeed not secure. The only known secure algorithm is the one known as "one-time pad", which is unconditionally secure. Hence proper approach is to design cryptography systems as "one-time pad" implementation. In one-time pad systems, main problem is key distribution. If security of keys is compromised, then security of system is compromised. Unfortunately, there is no full proof way of distributing keys securely using classical distribution techniques. The weekly introduced concepts "quantum cryptography" and "quantum key distribution" are potentially secure ways of solving distribution problem. Its strength stems from the laws of quantum physics. Proposed approach's security is unconditional as long as the laws of quantum physics stay valid.

Quantum Cryptography was invented by Charles Bennett and Gilles Brassard in 1984 [1]. It can be more properly termed as "Quantum Key Distribution (QKD)" because it allows two remote parties to generate a secret key guaranteed by quantum mechanics. This secret key is then used for encoding or decoding messages between two devices. Viewed in this light, since it is not the transmission of an encrypted message, it is the procedure of key distribution that is accomplished by quantum cryptography, QKD term is more appropriate.

The predecessor to the invention of QKD by Bennett and Brassard with the introduction of BB84 protocol in 1984 was Stephen Wiesner's concept of "quantum money" which is impossible to counterfeit [2]. Wiesner's idea was to "charge" dollar bill with several photons, polarized in two non-orthogonal bases. According to Heisenberg's uncertainty principle, there are quantum states which are incompatible in the sense that measuring one property necessarily randomizes the value of the other. So, to counterfeit a dollar bill, a counterfeiter must measure the states of all photons "trapped" in the bill and then reproduce them in his new bill. However, he do not know the initial bases in which the photons were coded (this information is kept in secret by the bank which produces these bills), so by measuring one of the properties (to say, vertical/horizontal polarizations) of a photon he randomizes the other (to say, left/right circular polarizations). It is obvious that this measurement will produce about 50% error. But the bank knows the right bases for each photon in the bill from the very beginning and thus it is capable of obtaining all of the information from this quantum system. It then compares the measured data with the data recorded in its database and makes a decision whether the bill was counterfeited or not. The idea of quantum money was brilliant, but it was also wholly impractical: it is impossible to store a photon trapped for a sufficiently long period of time. That's why Wiesner's article about quantum money was rejected in several scientific journals.

However, Bennett and Brassard thought of it in other way: rather to store the information, polarized photons can transmit it through a quantum channel. As a rule, this quantum channel is represented by an optical fiber – an ordinary single mode fiber often used in classical data transmission systems. The transmission is done by light pulses which are so weak that the probability of a photon appearing in each of the light pulses is considerably lower than one photon per pulse. The plot of the entire QKD system is to provide Alice and Bob with an identical sequence of random bits, which then can be used as a key to encrypt messages via one-time pad technique.

There are many research teams working in building and operating quantum cryptographic devices. Teams at Geneva, Los Alamos, IBM, Darpa are performing QKD through telecom fibers that can support distances up to about 70 km maximum through fiber, though at very low bit rates [3]. QKD setup applied in the studies of Darpa Network is given in Figure 1. Teams at Los Alamos [4] and Qinetiq [5] are performing free-space quantum cryptography, both through daytime sky and through the night at distances up to 23 km.

In addition to these efforts, whose systems all employ weak coherent quantum cryptography, there is also interest in cryptography based on a very different physical phenomenon, namely entanglement between pairs of photons produced by Spontaneous Parametric Down-Conversion (SPDC). This form of cryptography has been demonstrated by a research group in Geneva University [6].

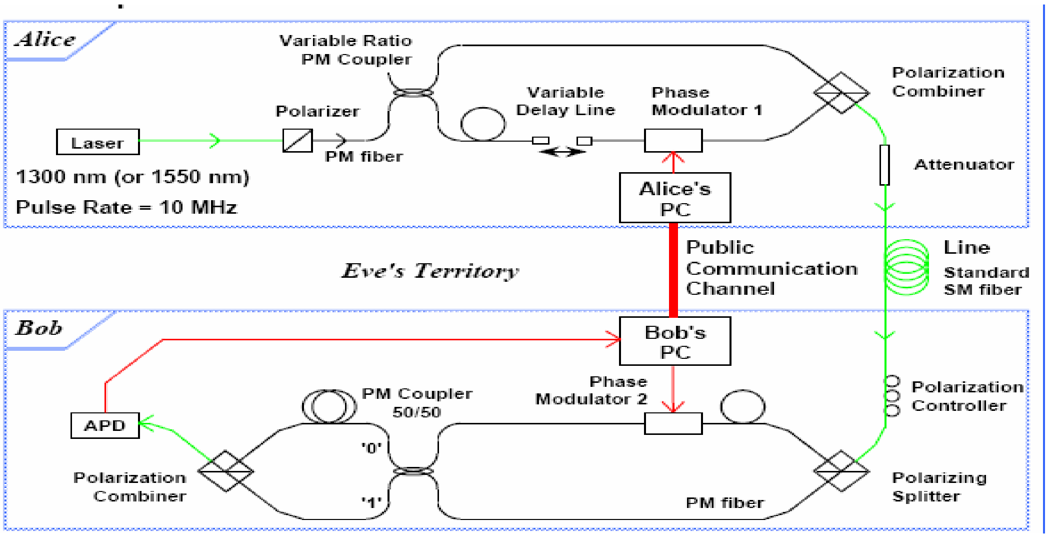

Figure 1 Darpa network QKD setup

If we look at the basics, in an ideal QKD system, a single photon is assumed to be used as an information carrier to distribute random keys. The QKD protocol utilizes the following rules stating physically disallowed tasks on such quantum system [7].

1) One can not simultaneously measure the two conjugate variables with arbitrary high accuracy.

2) One can not duplicate an unknown quantum state.

3) One can not take measurement of an unknown quantum state without perturbing the system.

These statements are different representations of the quantum mechanical complementarities and closely connected. For example, if one can duplicate an unknown quantum state, one can simultaneously measure the two conjugate variables with arbitrary high accuracy while preserving the unmeasured and unperturbed copy of the system.

Following the above quantum physics rules, single photons each having the responsibility of carrying a bit for key can be transmitted without any perturbation. After supplying the secure transformation of single photons, major issue is detecting these single photons. The ideal detector should fulfill the following requirements [8]:

- the quantum detection efficiency should be high over a large spectral range,

- the probability of generating noise, that is, a signal without an arriving photon, should be small,

- the time between detection of a photon and generation of an electrical signal should be as constant as possible, i.e., the time jitter should be small, to ensure good timing resolution,

- the recovery time (i.e., the dead time) should be short to allow high data rates.

In addition, it is important to keep the detectors practical. For instance, a detector that needs liquid helium or even nitrogen cooling would certainly render commercial development difficult. Unfortunately, it turns out that it is impossible to fulfill all the above criteria at the same time.

Avalanche Photo Diodes (APDs) are one of the detection components used in QKD systems. But they should be properly operated to achieve the best detection performance.

The objective of this master thesis is to build and test low temperature operation of an Avalanche Photo Diode (APD) for quantum cryptographic applications. An InGaAs APD will be used as the photon detection component. Low dark count is a required performance measure for the APD since as the dark count rate decreases detection efficiency increases. In order to decrease the dark count rate, detectors shall be sufficiently cooled. In our experiment for this purpose Thermo Electric Coolers (TECs) are going to be used. Cooled APD will be connected to an appropriate detection circuitry. Pulses detected by this circuitry will be amplified and monitored.

Chapter 2 gives information about Quantum Key Distribution. Details of the experimental setup and preliminary measurements performed before the experiment is covered in Chapter 3. Measures for the performance of the experiment are also given in this chapter. Experiment results are given in Chapter 4. Conclusions are presented in Chapter 5 and data sheets of components used in the experiment are given in the Appendices.

CHAPTER 2

QUANTUM KEY DISTRIBUTION

This chapter will give brief information about QKD and BB84 protocol which is the basic and first proposed QKD Protocol.

2.1 Basics of Quantum Key Distribution

QKD employs two distinct channels. One is used for transmission of quantum key material by very dim (single photon) light pulses. The other, public channel carries all message traffic, including the cryptographic protocols, encrypted user traffic, etc. as shown in Figure 2.

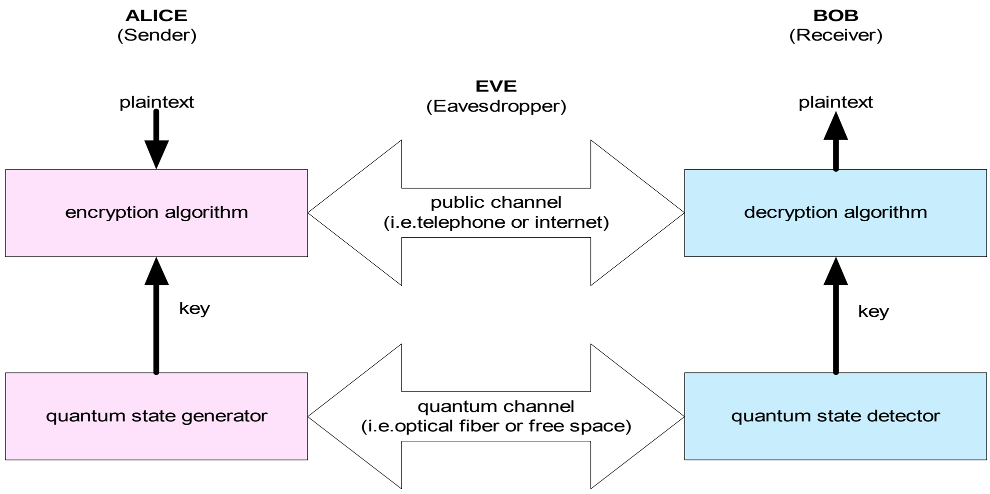

Figure 2 Quantum key distribution

QKD consists of the transmission of raw key material, e.g., as dim pulses of light from Alice to Bob, via the quantum channel, plus processing of this raw material to derive the actual keys. This processing involves public communication (key agreement protocols) between Alice and Bob, conducted in the public channel, along with specialized QKD algorithms. The resulting keys can then be used for cryptographic purposes, e.g., to protect user traffic. By the laws of quantum physics, any eavesdropper (Eve) that snoops on the quantum channel will cause a measurable disturbance to the flow of single photons. Alice and Bob can detect this, take appropriate steps in response, and hence foil Eve's attempt at eavesdropping.

2.2 BB84 Protocol

BB84 protocol was the first proposed protocol invented by Bennett and Brassard in 1984 to make use of quantum mechanics to exchange secret key over a quantum channel. The basic illustration of the protocol is given in Figure 3. Meanings of the used notations in the figure are as follows:

'+' represents the rectilinear scheme
'X' represents the diagonal scheme
'-' represents 0 (Horizontal polarization quantum state)
'/' represents 0 (45 degrees to horizontal polarization state)
'|' represents 1 (Vertical polarization quantum state)
'\' represents 1 (45 degrees to vertical polarization state)

As shown in figure, Alice sends a random sequence of photons polarized horizontal, vertical, right and left circular. Bob measures the photons polarization in a random sequence of bases, rectilinear and circular. Bob, then announces publicly which kind of measurement he made (but not the result of the measurement) and Alice tells him again publicly whether he made the correct measurement (i.e. rectilinear or circular). Alice and Bob then agree publicly to discard all bit positions for which Bob performed wrong measurement. Similarly, they agree to discard bit positions where Bob's detectors failed to detect the photon at all. The polarizations of the remaining photons is interpreted as "0" for horizontal or left circular and bit 1 for vertical or right circular. The resulting binary string should be shared as secret information between Alice and Bob.

As a result, QKD offers a technique for coming to agreement upon a shared random sequence of bits within two distinct devices, with a very low probability that other devices (eavesdroppers) will be able to make successful inferences as to those bits values. In specific practice, such sequences are then used as secret keys for encoding and decoding messages between the two devices employing "one-time pad" principles.

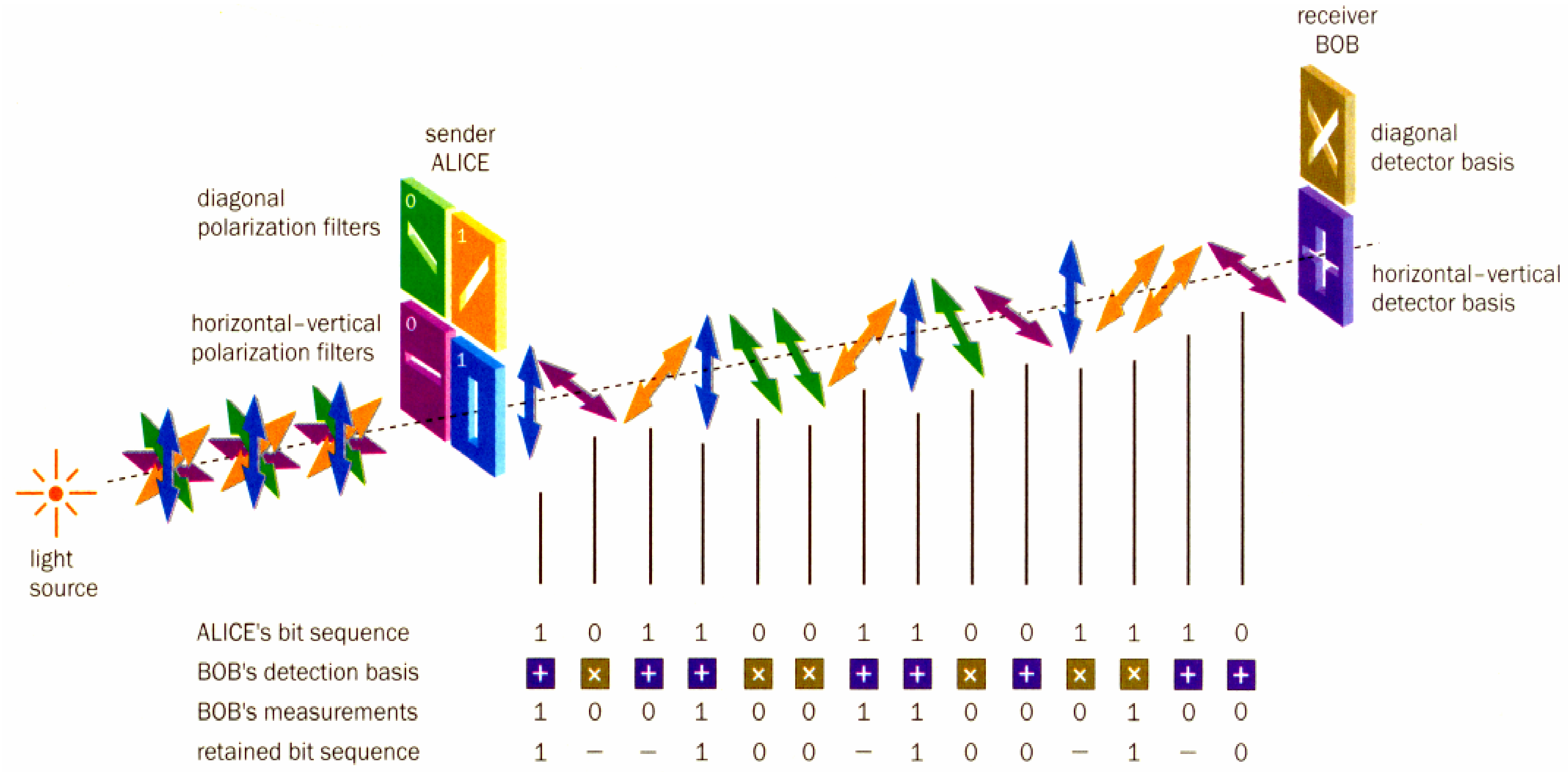

Figure 3 QKD protocol

2.3 Desirable properties for a QKD system

Some useful properties for a QKD system are as follows:

2.3.1 Confidentiality of Keys

Confidentiality is the main reason for interest in QKD. Public key systems suffer from an ongoing uncertainty that decryption is mathematically intractable. Thus key agreement primitives widely used in internet security architecture may perhaps be broken at some point in the future. This would not only hinder future ability to communicate but could reveal past traffic. Classic secret key systems have suffered from different problems, such as insider threats and the logistical burden of distributing keying material. Assuming that QKD techniques are properly implemented into an overall secure system, they can provide automatic distribution of keys that may offer security superior to classical approaches.

2.3.2 Authentication

QKD does not in itself provide authentication. Current strategies for authentication in QKD systems include prepositioning of secret keys at pairs of devices, to be used in hash-based authentication schemes, or hybrid QKD-public key techniques. Neither approach is entirely appealing. Prepositioned secret keys require some means of distributing these keys before QKD itself begins, e.g., by human courier, which may be costly and logistically challenging. On the other hand, hybrid QKD-public key schemes inherit the possible vulnerabilities of public key systems to cracking via unexpected advances in mathematics.

2.3.3 Sufficient Key Rate

One-time pad systems require keys of the same length as data files. Hence, key distribution systems must deliver keys fast enough so that encryption devices do not exhaust their supply of key bits. This is a race between the rate at which keying material is put into place and the rate at which it is consumed for encryption or decryption activities. QKD systems achieve on the order of 1,000 bits/second throughput for keying material, in realistic settings, and often run at much lower rates [9]. This is unacceptably low if one uses these keys in certain ways, e.g., as one-time pads for high speed traffic flows. However it may well be acceptable if the keying material is used as “session keys” for less secure (but often secure enough) algorithms such as DES or AES.

In any case, it is desirable to greatly improve upon the rates provided by today's QKD technology.

2.3.4 Robustness

This has not traditionally been taken into account by the QKD community. However, since keying material is essential for secure communications, it is extremely important that the flow of keying material not be disrupted, whether by accident or by the deliberate acts of an adversary. QKD provides a highly fragile service since QKD techniques have implicitly been employed along a single point-to-point link. If that link were disrupted, all flow of keying material would cease. Hence, a meshed QKD network is inherently far more robust than any single point-to-point link since it offers multiple paths for key distribution.

2.3.5 Distance and Location Independence

In the ideal world, any entity can agree upon keying material with any other (authorized) entity in the world. This feature is notably lacking in QKD, which requires the two entities to have a direct and dedicated path for photons between them, and which can only operate for a distance of a few tens of kilometers through fiber.

2.3.6 Resistance to Traffic Analysis

Adversaries desire to be able to perform useful traffic analysis on a key distribution system, e.g. a heavy flow of keying material between two points might reveal that a large volume of confidential information flows, or will flow, between them. QKD in general has weakness since most setups have assumed dedicated, point-to-oint QKD links between communicating entities. This clearly lays out the underlying key distribution relationships. However it is not clear how adversaries can use this information to their benefit. These considerations indicate that if properly implemented; QKD systems can provide secure communication between entities. The only problem remaining is finding ways of implementing a practical system. Hence; in the following chapters, principle components of such a system will be investigated to pave way to practical applications.

CHAPTER 3

EXPERIMENTAL SETUP

DARPA QKD system given in the introduction chapter and shown in Figure 1, has some basic components which are vital for QKD systems. These are:

- Single photon source
- Modulators for phase control and polarization combiners/splitters.
- Single photon detector

Among these, the most challenging component is the single photon detector. It is a key component in a QKD system which influences both the key creation rate and the error rate. In order to obtain the optimum detection efficiency, dark count rate should be kept as low as possible. This requires low temperature operation of APD. Since the objective of this study is to investigate detectors suitable for QKD applications, experimental studies are devoted to single photon detecting hardware. Following sections of this chapter will give detailed information about the major equipment and circuitry of this setup; APD, TEC, Laser, Amplifier and Detection circuitry connected to the APD.

In our experiment the setup shown in Figure 4 is established. APD is used as the detection component. Pulsed semiconductor laser diode and APD are driven by a pulse generator. These pulses are fed into an attenuator via optical fiber and detected by APD. Detected signals are amplified and measured.

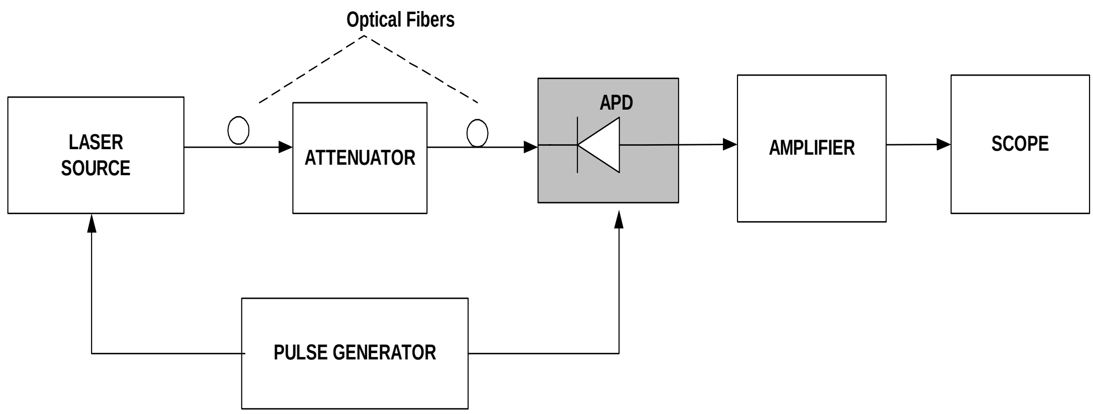

Figure 4 Experimental setup

3.1 Avalanche Photo Diode

With the availability of single-photon and photon-pair sources, the success of QKD essentially depends on the ability to detect single photons. In principle, this can be achieved using a variety of techniques, for instance, photomultipliers, avalanche photodiodes, multichannel plates, and superconducting Josephson junctions. If APDs are well developed, they are a good choice for single photon detection.

Three different semiconductor materials are used for APDs: silicon, germanium, or indium gallium arsenide, depending on the wavelengths. Figure 5 shows quantum efficiencies obtained for different detectors [10]. Silicon APDs exhibit very good performance between 600 and 900 nm: quantum efficiencies for detecting single photons around 60%, dark counts in the absence of light below 100 counts per second and sub-nanosecond timing resolution. The excellent performance of silicon APDs has enabled significant progresses in luminescence studies, astronomy, sensor applications and fundamental research in physics. However, for photon counting at the longer telecom wavelengths of 1300 nm and 1550 nm, the situation is no longer so easy. Although near-infrared photomultiplier tubes having a spectral response extending to 1700 nm exist, their quantum efficiency does not exceed a fraction of a percent.

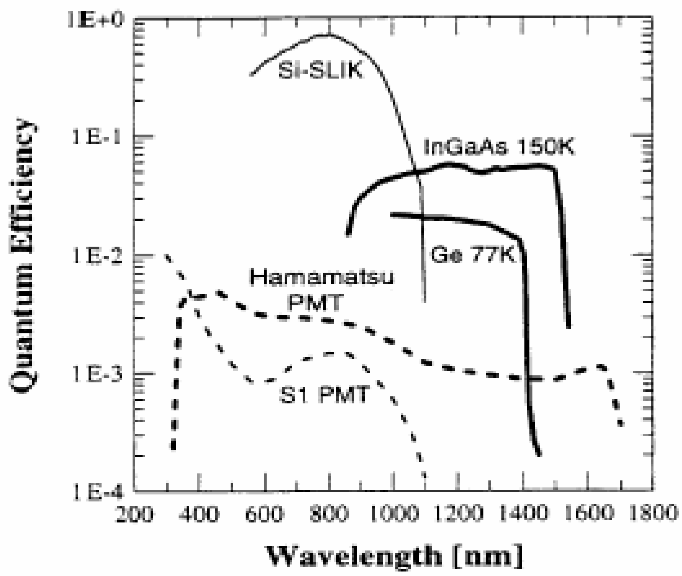

Figure 5 Quantum efficiencies of various detectors

For 1300 nm photons, germanium APDs have been extensively studied. In order to have a reasonable dark count rate, these detectors must be cooled, usually with liquid nitrogen, to a temperature below 150 K, making them impractical for most applications. Furthermore, the cut-off wavelength of these APDs when cooled is around 1450 nm, making them unsuitable for use as photon counters for 1550 nm photons.

The 0.73 eV bandgap of InGaAs, lattice matched to an InP substrate makes single-photon sensitivity possible up to a wavelength of 1650 nm. So InGaAs/InP APDs, originally developed for optical communication applications, for photon counting at 1300 nm and 1550 nm became commercially available.

3.2.1 APD Structure

An avalanche photodiode (APD) is basically a p-i-n diode specifically designed for providing an internal current gain mechanism. When reverse biased, the APD is able to sustain a large electric field across the junction. An incoming photon is absorbed to create an electron-hole pair. The charge carriers are then swept through the junction and accelerated by the strong electric field. They can gain enough energy to generate secondary electron-hole pairs by impact ionization. These pairs are in turn accelerated and can generate new electron-hole pairs. This multiplication phenomenon is known as an avalanche.

In the case of InGaAs/InP APDs, the photons are absorbed in a narrow bandgap InGaAs layer as seen in the Figure 6.

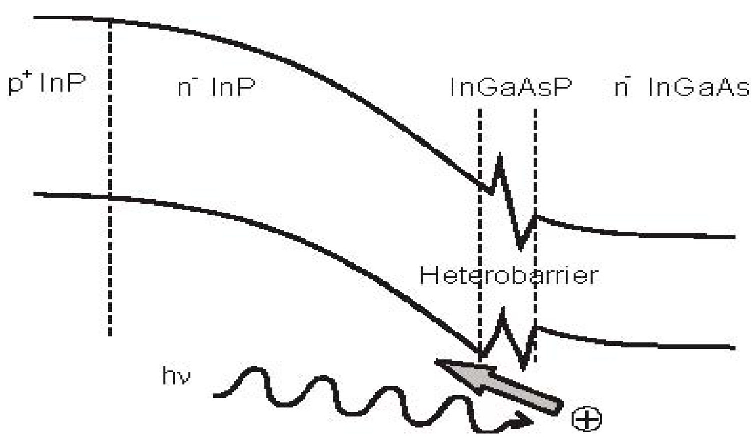

Figure 6 Structure of InGaAs/InP APD

The photo generated hole is then injected into the wider bandgap InP multiplication layer. Separate absorption and multiplication layers are designed to optimize the avalanche behavior and minimize the excess noise factor associated. This also ensures that tunneling breakdown in the narrow bandgap InGaAs layer occurring at field values lower than the threshold for avalanche multiplication does not impair functioning. Because of the bandgap difference between InGaAs and InP, a grading quaternary InGaAs layer is used to smooth the band discontinuity, which could otherwise trap charge carriers and slow down timing response.

3.2.2 Geiger Mode Operation of APD

Geiger mode operation is one of the basics in quantum cryptography for single photon detection when utilizing the features of an APD. It increases the detector efficiency significantly. The general idea is to temporarily displace the electrical equilibrium inside the APD.

In Geiger mode operation, the reverse voltage applied is below the so-called breakdown voltage, the point where a self-sustaining avalanche current can be initiated by thermal fluctuations or tunneling effects. The output signal is a linearly amplified copy of the input signal. Figure 7 represents the I-V characteristics of an APD and illustrates how single-photon sensitivity can be achieved. The APD is biased, with an excess bias voltage, above the breakdown value and is in a metastable state (point A). It remains in this state until a primary charge carrier is created. In this case, the amplification effectively becomes infinite, and even a single-photon absorption causes an avalanche resulting in a macroscopic current pulse (point A to B), which can readily be detected by appropriate electronic circuitry. This circuitry must also limit the value of the current flowing through the device to prevent its destruction and quench the avalanche to reset the device (point B to C). After a certain time, the excess bias voltage is restored (point C to A) and the APD is again ready to detect a photon.

The actual value of the breakdown voltage depends on the semiconductor material, the device structure and the temperature. For InGaAs/InP APDs, it is typically around 50V.

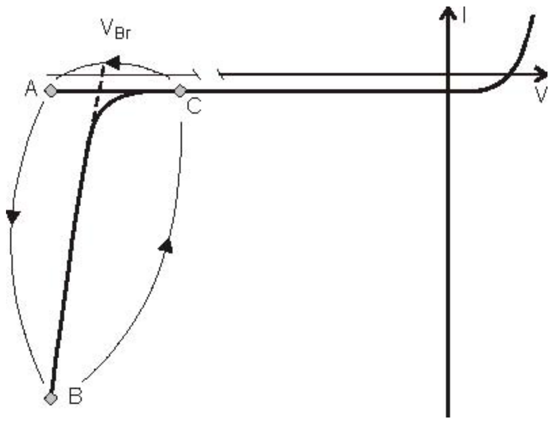

Figure 7 I-V curve of APD

To reset the APD, this macroscopic current must be quenched, the emission of charges must be stopped and the diode recharged. Three main possibilities exist:

1) Passive-quenching circuits: A large (50–500 kΩ) resistor is connected in series with the APD. This causes a decrease in the voltage across the APD as soon as an avalanche starts. When it drops below breakdown voltage, the avalanche stops and the diode recharges. The recovery time of the diode is given by its capacitance and by the value of the quench resistor. The maximum count rate varies from a few hundred kilohertz to a few megahertz.

2) Active-quenching circuits: Bias voltage is actively lowered below the breakdown voltage as soon as the leading edge of the avalanche current is detected. This mode makes possible higher count rates than those in passive quenching (up to tens of megahertz), since the dead time can be as short as tens of nanoseconds. However, the fast electronic feedback system makes active-quenching circuits much more complicated than passive ones.

3) Gated-mode operation: Bias voltage is kept below the breakdown voltage and is raised above it only for a short time, typically a few nanoseconds when a photon is expected to arrive. Maximum count rates similar to those in active-quenching circuits can be obtained using less complicated electronics. While several biasing modes have been proposed and tested, the best performance in the case of InGaAs/InP APDs is obtained with gated operation. Two such gate pulses are separated by a longer hold-off

time, during which the bias voltage is kept well below the breakdown voltage. Because of the possibility of applying a high excess bias voltage, this technique makes it possible to achieve high detection efficiencies and good timing resolutions. In addition, the fact that the detector is activated only for a short time period, allows to limit afterpulse effects and to discriminate photo-counts from noise counts which are not coincident. Gated mode operation can also be used in a scanning mode, to investigate the profile of the arrival time of photons.

The basic circuit configuration for the Geiger mode operation is shown in Figure 8. The APD is reverse biased V_R and the signal is read out over a resistive load and amplified. Using the pulse generator the bias can be further increased for short duration of time.

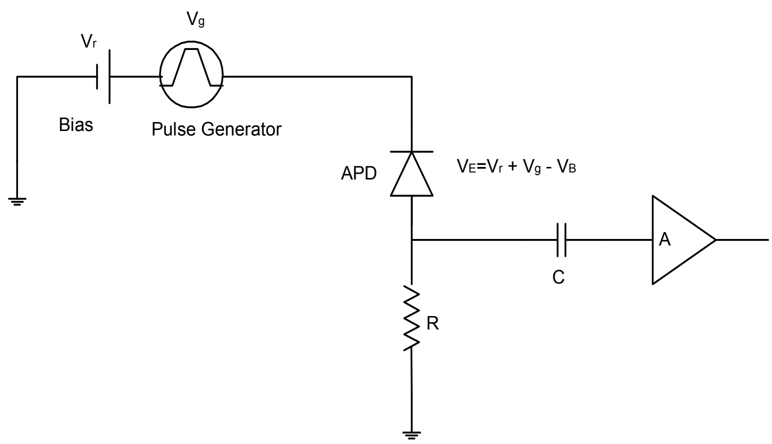

Figure 8 Circuitry of Geiger mode operation

Figure 9 shows parameters characterizing the Geiger mode operation. Rising and falling times of the edges are neglected. Detection of single photon is done inside the gate window.

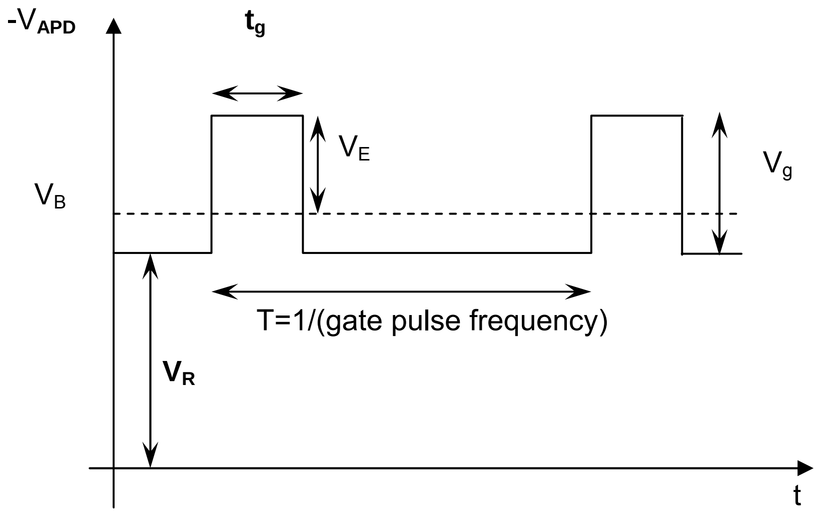

Figure 9 Voltage-time parameters

Where,

V_R	The reverse bias of the APD
V_B	Breakdown voltage of the APD
V_E	Excess voltage above V_B from the gate pulse
V_g	Amplitude of the gate pulse
t_g	Width of the gate pulse (detection window)

3.2.3 Breakdown Voltage Measurement

By increasing the APD bias, Breakdown Voltage (V_B) will ultimately be reached. Above this limit the gain is infinite and an unlimited current will flow through the APD, probably exceeding the absolute maximum ratings, if not by some means controlled. Normal operation is therefore below V_B, yielding a limited gain. Above V_B dark current carriers will instantly be picked up by the e-field and transported to the multiplication region.

In order to achieve breakdown, carriers must be present in the depletion region. If not, it would not be possible to operate the APD above V_B simply because there had been nothing to multiply. However dark current carriers always exists and Geiger Mode operation avoids operating the APD above V_B in such short period of time that the probability of a dark current carrier being multiplied is small.

EG&G C30644 APD is used in our experiment and as specified in the data sheet of the APD given in Appendix A, breakdown voltage for this APD is 60 V.

In order to measure the breakdown voltage of the APD experimentally, the setup shown in Figure 10 is established.

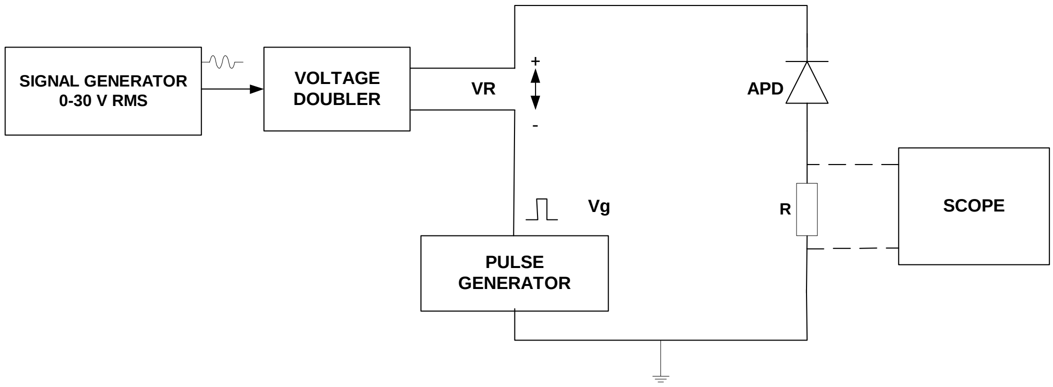

Figure 10 APD breakdown voltage measurement setup

As shown in Figure 10 APD is reverse biased by a DC voltage with its breakdown voltage (60 V). Since we didn’t have a high voltage source, a signal generator followed by a voltage doubler circuitry is used for this purpose and sufficient voltage is obtained.

Pulse Generator is used to operate the APD in gated mode so that an avalanche will occur at the APD when the bias voltage across the APD is greater than the breakdown voltage. As the bias voltage decreases below the breakdown voltage, APD will quench. Pulse Generator voltage is increased and by monitoring the voltage across the resistor R = 330 KΩ, breakdown voltage is measured. Measurement results are given in Figure 11 and Figure 12.

Figure 11 Measurement results as the avalanche starts

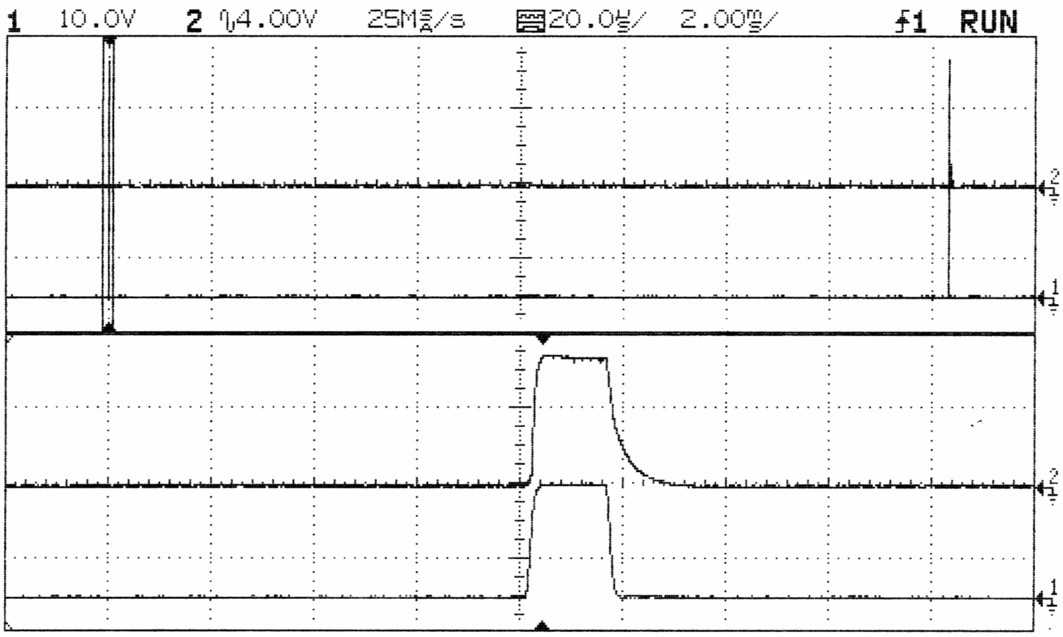

Figure 12 Measurement results for the increased bias voltage

For the plots in the above figures, Channel 1 shows the input pulse signal and Channel 2 shows the voltage across the resistor. Lower plots show the details of the selected region of the upper plots.

Start of the avalanche is seen in Figure 11 where the output is on the order of 0.4 V. The ripples can be easily seen at the duration of gate caused by the avalanche. In the Figure 12, pulse signal is kept constant and DC bias is changed, as the bias changes since the magnitude of the excess voltage so the ionization increases the current passing across the APD increases.

Tektronix TM503 0-15 V Pulse Generator, Advance Instruments Signal Generator and HP 54616B Oscilloscope are used in this experiment.

3.2.4 Dark Current

A major noise parameter in an APD is the dark current. Even though no light is present some current will still flow between the terminals of the device. The magnitude of this current differs, dependent on fabrication. Dark current arises from random electron-hole pair generated thermally or by tunneling. A dark current generated electron will have the same effects as a photo generated one, thereby multiplication. Tunneling is mostly a matter of design and choice of materials. It is therefore not a process the user can alter by some means of external stress, unless compromising vital properties like bias. However thermally generated carriers can obviously be controlled by the temperature. The rate of thermally generated carriers in an intrinsic material is given by

$$g(T) = \alpha_r n_i^2(T) \tag{3.1}$$

Hence g (T) exhibits dependency, decreasing with less temperature and vise versa. By reducing the temperature the dark current can be decreased significantly. The dark current in an APD can be given by

Where α_r is consant of proportionality and,

$$n_i(T) = 2\left(\frac{2\pi kT}{h^2}\right)^{3/2} (m_n^* m_p^*)^{3/4} e^{-E_g/2kT} \tag{3.2}$$

$$I = \frac{dQ}{dt} \tag{3.3}$$

$$= \frac{nq}{\Delta t}$$

Where q is the electronic charge (1,6. 10 $^{-19}$ C), n is the number of electrons and T is a time interval with a scale of ns. The number of electrons passing a cross section per ns is

$$n = \frac{I.\Delta t}{q} \tag{3.4}$$

$$= 6.26.10^{9}.I$$

In order to achieve less than one electron per ns the dark current must be in the sub-nanoamper range.

3.2.5 Temperature Dependence of APD

An APD is a device similar to a rectifier diode, except its output current contains a term which is dependent on the incident light intensity on its surface in the operating wavelength range. The APD output current is given by

$$I_{APD} = -I_d + I_s\left(e^{\frac{qV}{kT}} - 1\right) \tag{3.5}$$

where I_{APD} is the APD output current, I_d is the detected photo-current, I_s is the saturation dark current, q is the electron charge, V is the device bias voltage (negative for reverse bias), k is Boltzmann's constant, and T is the temperature. The second term of this equation represents the APD dark current and the first term, I_d, represents the photo-current, given by

$$I_d = \Re.P \tag{3.6}$$

where is the APD responsivity, and P is the incident optical power. The APD responsivity, R (A/W), is obtained from

$$\Re = \eta G.\frac{q}{hc}\lambda \tag{3.7}$$

where η is the wavelength dependent quantum efficiency, G is the APD internal gain, h is Planck's constant, c is the speed of light, and λ is the wavelength of the incident light. At a constant bias voltage, the APD operating temperature affects its output current. The APD gain, and therefore its responsivity, is a strong function of the device temperature. On the other hand, the APD dark current, as well as the dark current noise, is also dependent on the APD temperature.

At a constant bias voltage and wavelength, the APD responsivity increases by decreasing the device temperature. Therefore, cooling the APD is recommended to increase its detected photo-current. The APD dark current, given by the second term of the current equation, is also dependent on the device operating temperature. Decreasing the APD temperature will increase the dark current. The maximum dark current will be obtained at a temperature of 0 K and will be equal to the saturation current. More importantly, the APD dark current is associated with noise, known as the dark current shot noise, which is given by

$$i_n^2 = 2qGFB\left[I_s \left(e^{\frac{qV}{kT}} + 1 \right) + I_d \right] \tag{3.8}$$

I_n is the shot noise current, F is the excess noise factor, and B is the device bandwidth. The APD temperature affects the dark current shot noise directly in the denominator of the exponential power and indirectly by its effect on the device gain. The first effect is dominant; and for a reverse bias voltage, the dark current shot noise is reduced by reducing the operating temperature.

In most applications, the effect of the APD dark current on the output signal can be eliminated by either modulating the input optical signal or by subtracting the dark current from the device output. Therefore, low temperature operation of APDs is recommended in order to increase the device responsivity and to reduce the dark current shot noise.

3.3 Thermo Electric Cooler

A thermoelectric cooler consists of an array of semiconductor (group V-VI, e.g. bismuth telluride) pellets that have been positively (p) or negatively (n) doped. The p-n pellet pairs are connected electrically in series and thermally in parallel [11]. Consider a simple thermoelectric cooling unit, as illustrated in Figure 13, in which the electrical resistance between the semiconductor elements and metal links, as well as the resistances of the links themselves, are negligible. Also, the thermal resistance between the semiconductor pair, the heat source, and the heat sink are neglected. For simplicity, all of the material thermal coefficients are assumed constant and independent of temperature.

3.3.1 TEC Theory of Operation

TEC operation is based on the Peltier effect which results in the transport of heat when electric current flows in a conductor. This heat flow is revealed only at a junction between two different materials where the heat transport on either side is different.

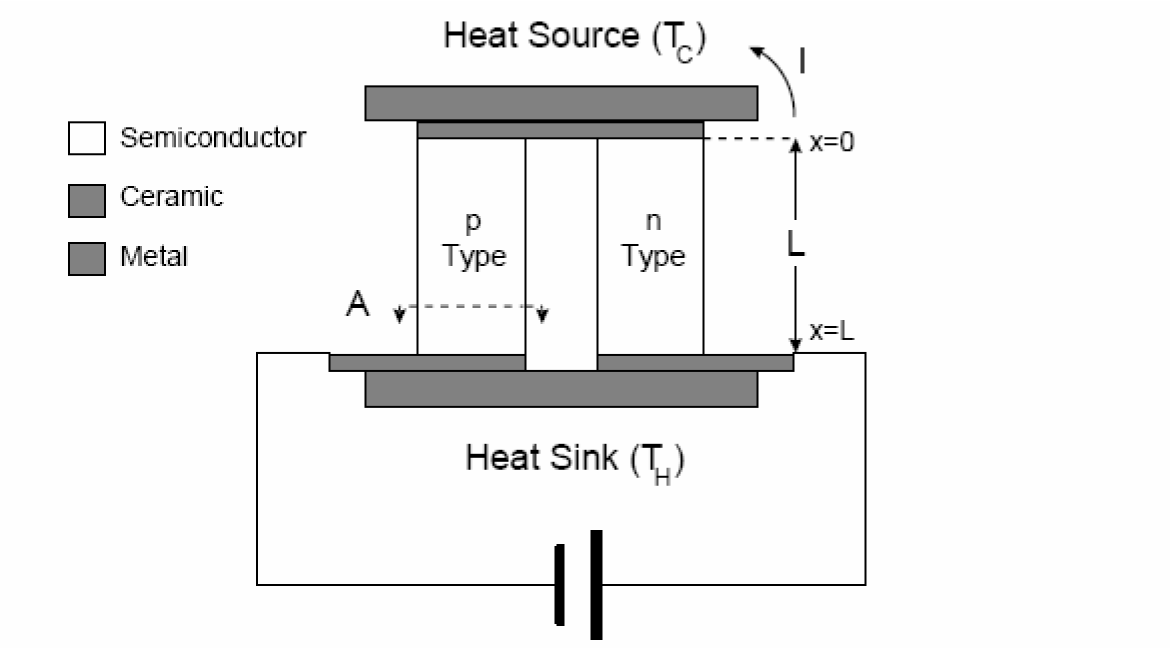

Figure 13 A TEC p-n pair

The TEC cooling cycle can be further understood in a qualitative manner by studying the energy band diagram of its materials, as shown in Figure 14. An electron at the cold metal absorbs a heat quanta, which leads to an increase in the electron's potential energy. The applied electric field from the supply causes the electron to drift to the n-material. A fraction of the electron energy is converted to kinetic energy as the electron proceeds through the n-material. At the end of the n-material, the electron rejects its energy gain to the hot metal in the form of heat. In order to complete the cycle, the electron must reject more energy to pass through the p-material using the lower band. On the other hand, at the p-material cold-metal junction, the electron gains more energy, through heat absorption, in order to complete its cycle.

Similarly, the holes do the same thing in the opposite direction, which leads to a heat transfer from the cold metal to the hot metal by both charge carriers. The power supply must provide the energy for the carriers to continue the cycle and also provide the system with the energy that is lost due to the electrical resistance of the cooling unit.

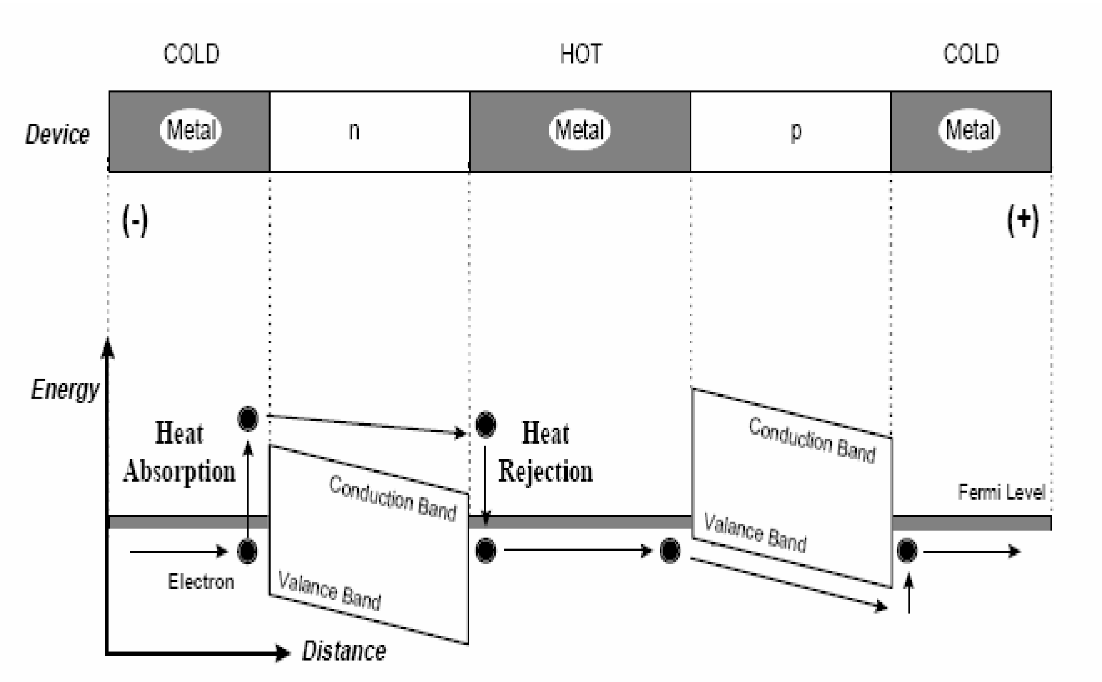

Figure 14 Energy band diagram for a thermoelectric cooling unit

3.3.2 Heat Loads

Physical view of a TEC is shown in Figure 15. The heat loads at the cold side of the TEC cooler are due to active and passive heat sources. TEC passive heat loads come from the temperature gradient between the cooled components and the ambient environment. Passive heat loads are:

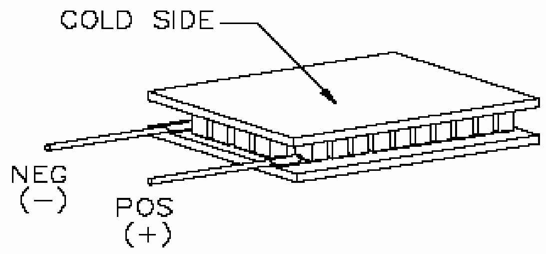

Figure 15 Physical view of a TEC

1) Radiation Heat: The first passive load, Q_{RAD}, is the heat radiation from the ambient environment to the TEC cold side.

   When two objects at different temperatures come within proximity of each other, heat is exchanged. This occurs through electromagnetic radiation emitted from one object and absorbed by the other. The hot object will experience a net heat loss and the cold object a net heat gain as a result of the temperature difference. This is called thermal radiation. Radiation heat loads are usually considered insignificant when the system is operated in a gaseous environment since the other passive heat loads are typically much greater in magnitude. Radiation loading is usually significant in systems with small active loads and large temperature differences, especially when operating in a vacuum environment.

   The fundamental equation for radiation loading is:

$$Q_{RAD} = F.e.s.A_{TEC}\left(T_{amb}^4 - T_C^4\right) \tag{3.9}$$

   Where,

   F: surface shape factor (worst case value is 1)

   e: surface emissivity (worst case value is 1)

   s: Boltzmann constant (5.667 X 10^{-8}W/m^{2}K^4),

   A_{TEC} : area of the TEC cold surface (m^2), and

   T_{amb} : ambient temperature (K).

   <u>Example Calculation</u>: If a charge coupled device is being cooled from an ambient temperature of 27°C (300K) to -50°C (223K).

The known parameters are; the detector surface area (includes 4 edges + top surface) is 8.54 X 10 -4 m2 and has an emissivity of 1. Assume the shape factor = 1

From the equation above;
Q_{RAD} = (1)(1) (5.66X10^{-8} W/m^2K^4) (8.54 X 10-4 m^2) [(300 K)^4 - (223 K)^4] = 0.272 W

2) Conductive Heat: The second passive load Conductive Heat, Q_{CON}, is due to the conduction between the TEC cold surface and the ambient environment through the air space below the package window, which has a length L_P.

   Conductive heat transfer occurs when energy exchange takes place by direct impact of molecules moving from a high temperature region to a low temperature region.

   Conductive heat loading on a system may occur through lead wires, mounting screws, etc., which form a thermal path from the device being cooled to the heat sink or ambient environment.

   The fundamental equation which describes conductive loading is:

$$Q_{CON} = \frac{K_{Air} A_{TEC}}{L_P}(T_{amb} - T_C) \qquad (3.10)$$

   where K_{air} is the air thermal conductivity (W/m °C). Typical value for K_{air} / L_p is 21.7 w/m^2C for a flat, horizontal plate in air at 1 atm.

   <u>Example Calculation</u>: A square plate is being cooled from 25°C to 5°C. The top and four sides are exposed surfaces. The plate is 0.006 meters thick and each side is 0.1 meters long.

   From the conduction equation:

   Q_{CON} = (21.7 w/m^2C (0.0124 m^2)(25°C - 5°C) = 5.4 watts

   At the TEC hot side, heat accumulation will lead to device failure. Therefore, a heat sink is used for heat dissipation to the ambient environment. Considering the worst-case situation in which the heat transfer from the heat sink to the ambient environment is only through radiation, the amount of heat radiated from the heat sink, Q_{HS}, is given by

$$Q_{HS} = F.e.s.A_{HS}\left(T_H^4 - T_{amb}^4\right) \tag{3.11}$$

where A_{HS} is the heat sink surface area.

Active heat loads are heat loads due to APD and thermistor indicated as $Q_{APD}$and Q_{THR} respectively. The power consumed in these elements is directly transformed to heat and is given, respectively, by

$$Q_{APD} = V_{BIAS}.I_{APD} = V^2{}_{BIAS} / R \tag{3.12}$$

For example, a typical lead selenide (PbSe) infrared detector is operated at a bias voltage of 50 volts and a resistance of 0.5 megohms. The active load therefore, is .005 watts.

$$Q_{THR} = \frac{R_T}{\left(R_T + R_S\right)^2} V_Z^2 \tag{3.13}$$

Where, for a thermistor, the relation between its resistance (R_T) and the temperature (T) can be given by [11]

$$\mathrm{R_T} = 10^4 \exp\left[3940\left(\frac{1}{\mathrm{T}} - \frac{1}{298}\right)\right] \tag{3.14}$$

3.3.3 Heat Estimation for a Thermoelectrically Cooled APD

In order to estimate the amount of heat to be transferred while cooling the APD, heat generation by APD (Q_{APD}) and thermistor (Q_{THR}) should be considered. Conductive heat (Q_{CON}) and Radiative heat are also important. In our case, since insulation is used, radiative heat is negligibly small.

The heat transfer problem of a thermoelectric cooling is summarized in the power flow diagram of Figure 16 where P is the internal power of the TEC, Qc is the total of heat sources and Qs is the total of heat sources and internal heat of the TEC (P). Q_{HS} is the heat transferred to the heat sink.

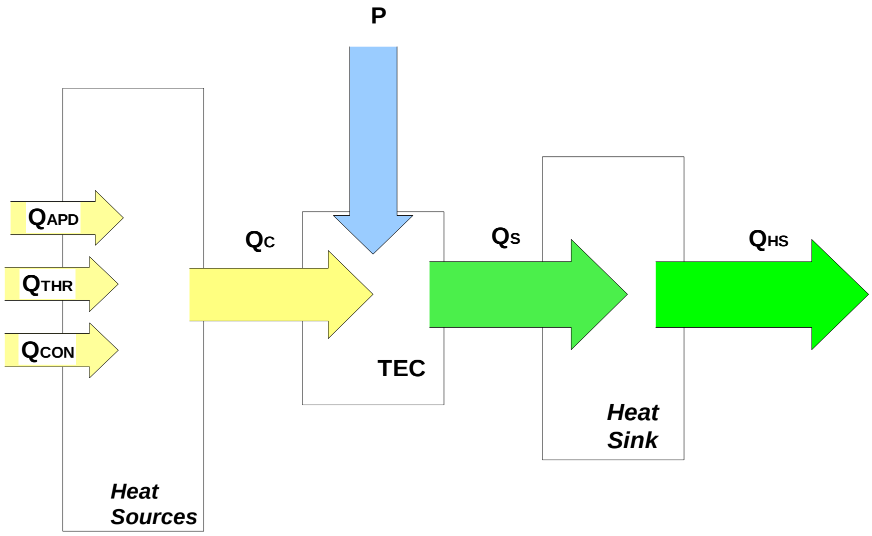

Figure 16 Power flow diagram for the APD cooling system

3.3.4 APD Cooling Assembly

Cooling operation of APD using TECs requires a carefully designed box which provides housing for APD and TECs. This box should provide In order to understand and analyze the cooling performance of TECs and obtain the minimum reachable operating temperature, the setup shown in Figure 17 is established.

Setup is composed of an APD box, a heat sink placed below the box, a fan, DC power supplies for fan, coolers in the box and the other measurement equipment.

APD assembly inserted in a copper block is shown in Figure 18. In order to provide exact alignment of the fiber, a copper block is drilled in the dimensions of the APD. APD is first placed in a plastic housing, and then located into the hole. At the opposite side, there is also a plastic material having a hole just enough to let passing a fiber. This arrangement supported the healthier operation with APD and the fiber.

The distance between the end of the fiber and the APD window is also affecting the output signal.

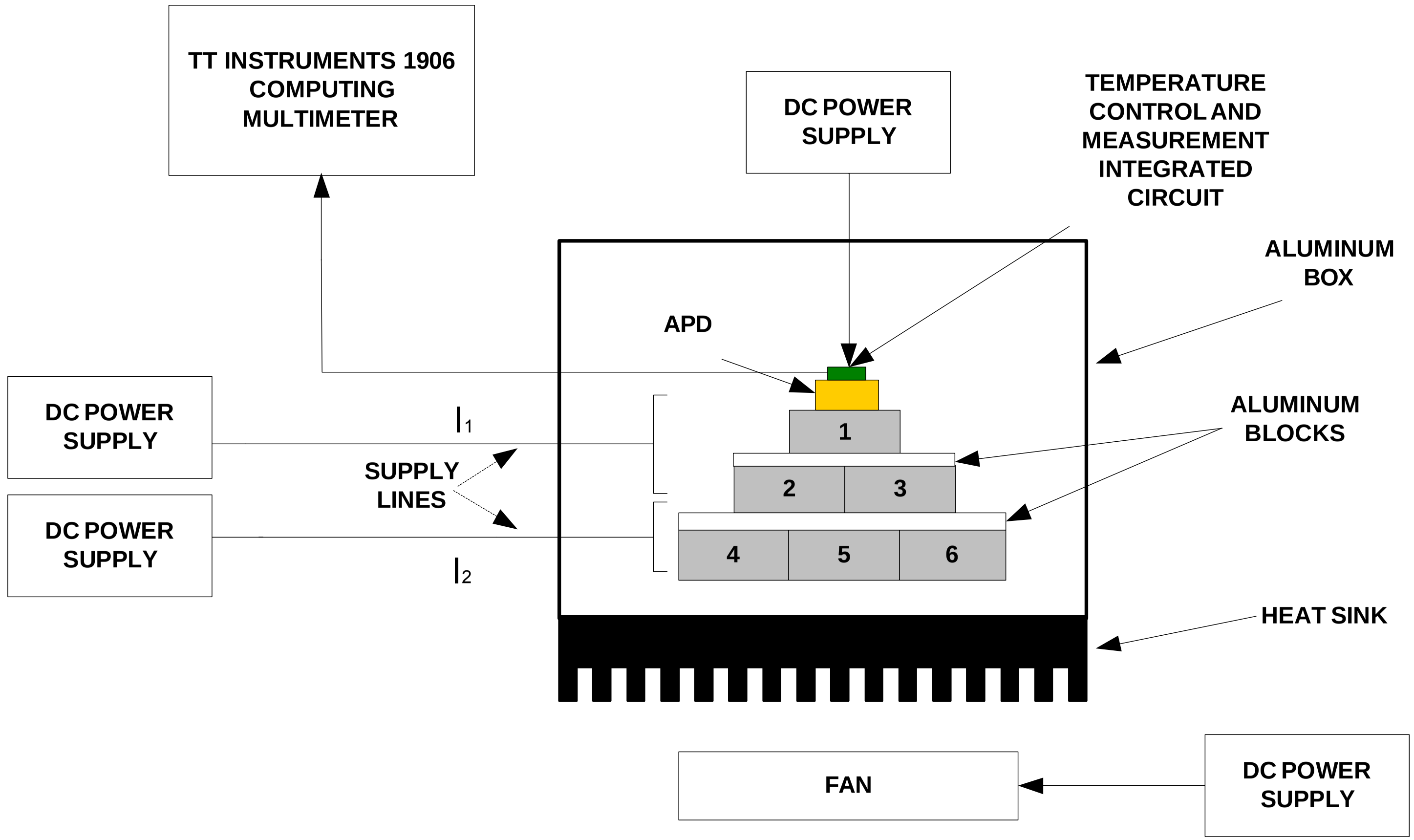

Figure 17 Temperature measurement setup

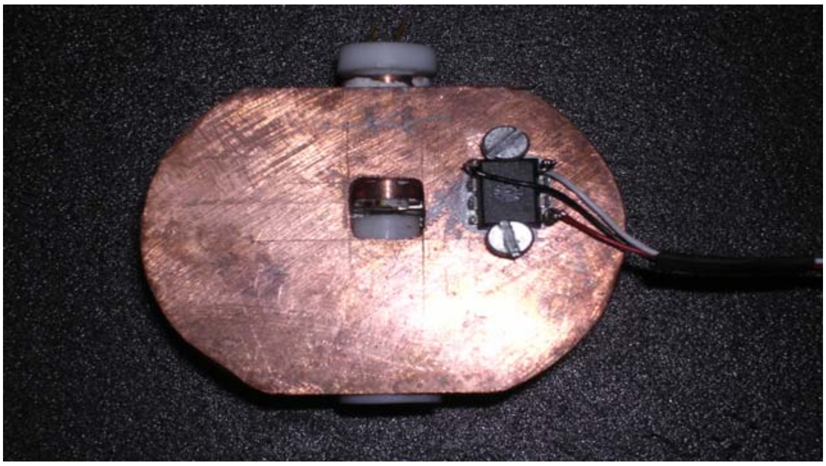

Figure 18 APD assembly

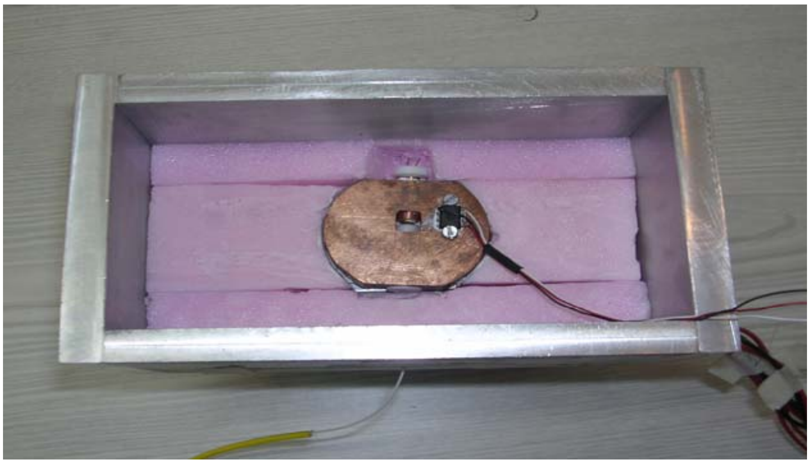

Figure 19 Upper view of APD box

Figure 20 Side view of APD box

APD assembly is inserted in a box. The housing of the APD box is aluminum. At the center of the box rest the TEC layers (3 layers). APD inserted in a copper block is mounted on these layers. Between each layer an aluminum block is placed so that a smooth heat transfer occurs. Box is filled with foam in avoid to cold heat leakage. APD box upper and side view is shown in Figure 19 and Figure 20 respectively.

The hot side of the bottom layer of TECs is placed on a brass heat sink. A fan placed near the box is used to cool the heat sink.

Electrical leads for temperature control and measurement integrated circuit, TEC and APD cables pass from the openings of the box.

To measure the APD package temperature, a temperature control and measurement integrated circuit is placed above the APD package. TMP01FP, from Analog Devices, is used. It is a temperature sensor which generates a voltage output proportional to absolute temperature and a control signal from one of the two outputs when the device is either below or above a specific temperature range. But we just used the integrated circuit to measure the temperature. The data sheet for the controller is given in Appendix B.

Upper TECs are numbered as 1,2,3 and supplied by a current of I_1, TECs at the lower layer are numbered as 4,5,6 and supplied by a current of I_2,

Previous experimental tests of each TEC showed that operating the cooler with a bias current of approximately 1-1.4 A is sufficient. So for this temperature measurements, I_1 is adjusted to 3.5 A and I_2 to 4 A. When the power flow of the APD cooling system is considered, I_2 should be greater than the $I_{1.}$ For these conditions a minimum operating temperature of **- 25ºC** is reached.

For the case of reached minimum temperature of -25 ºC, power estimation can be made as follows:

APD has a maximum power dissipation of 20 mW as obtained from the data sheet of the APD,

$$Q_{APD} = 20 \text{ mW}$$

Instead of thermistor, temperature control and measurement integrated circuit is used. Integrated circuit is biased by 5 V and maximum output current is 2 mA so

Q_{IC} = 5V. 2 mA = 20 mW

From $Q_{RAD} = F.e.s.A_{TEC}\left(T_{amb}^4 - T_C^4\right)$, where F and e is 1 for the worst case, s= 5.667 X 10^{-8} A_{TEC} = 48 mm^2 and T_{amb} = 27 ºC (300 K), T_c=-25 ºC (248 K).

Q_{RAD} = 5.667 X 10^{-8}. 48. 10^{-4}. (300^4-248^4) = 23 mW

So the total heat load is

Q_c = 20 + 20 + 23 = 63 mW

3.4 Laser Source

Optical quantum cryptography is based on the use of single-photon states. Unfortunately, these states are difficult to realize experimentally. Practical implementations rely on faint laser pulses or entangled photon pairs, in which both the photon and the photon-pair number distribution obey Poisson statistics. Hence both possibilities suffer from a small probability of generating more than one photon or photon pair at the same time. For large losses in the quantum channel, even small fractions of these multi-photons can have important consequences on the security of the key. Entangled photon pairs generated by Spontaneous Parametric Down Conversion (SPDC) are in the out of this thesis scope and will not be explained. In this section, lasers will be briefly discussed as a single-photon source.

3.4.1 Statistics of the Pulse

There is a very simple solution to approximate single photon states: coherent states with an ultra low mean photon number μ (≈ 0.1). They can easily be realized using only standard semiconductor lasers and calibrated attenuators. The probability of finding *n* photons in such a coherent state follows the Poisson statistics:

$$P(n,\mu) = \frac{\mu^n}{n!} e - \mu \qquad (3.15)$$

Accordingly, the probability that a nonempty weak coherent pulse contains more than one photon,

$$P(n > 1|\ n > 0, \mu) = \frac{1 - P(0,\mu) - P(1,\mu)}{1 - P(0,\mu)} \tag{3.16}$$

$$= \frac{1 - e^{-\mu}(1+\mu)}{1 - e^{-\mu}} \cong \frac{\mu}{2}$$

can be made arbitrarily small. Weak pulses are thus extremely practical and have indeed been used in the vast majority of experiments. However, they have one major drawback. When μ is small, most pulses are empty: $P(n = 0 \approx 1 - \mu$. In principle, the resulting decrease in bit rate could be compensated for thanks to the achievable gigahertz modulation rates of telecommunications lasers. But in practice, the problem comes from the detectors' dark counts (i.e., a click without a photon's arriving). Indeed, the detectors must be active for all pulses, including the empty ones. Hence the total dark counts increase with the laser's modulation rate, and the ratio of detected photons to dark counts (i.e., the signal-to- noise ratio) decreases with μ. The problem is especially severe for longer wavelengths, at which photon detectors based on indium gallium arsenide semiconductors (InGaAs) are needed, since the noise of these detectors explodes if they are opened too frequently (in practice with a rate larger than a few megahertz). This prevents the use of really low photon numbers, smaller than approximately 1%. However, it is important to stress that there is an optimal μ depending on the transmission losses. After key distillation, the security is just as good with faint laser pulses as with single-photon states. The price to pay for using such states is a reduction of the bit rate.

Most experiments have relied on μ = 0.1, meaning that 90.48% of pulses contain no photon, 9.05% of pulses contain one photon, 0.45 of pulses contain two photons, 0.002%of pulses contain three photons, etc. At the expense of more than 90% of pulses being empty, we thus generate one-photon pulses with a total fraction of multi-photon pulses smaller than 0.5%.

The multi-photon pulses can cause problems, though. If pulses contain two or more photons in the same quantum state, this would allow eavesdropper to retain one of these photons and perform their measurement without revealing their presence.

This potentially leaked information must be taken account and eliminated by means of privacy amplification.

Another issue is that most pulses sent will be empty. Even if that can be compensated for by using higher pulse frequencies, Bobs detectors still have to be gated whenever a pulse is sent, increasing the chances of recording a so called dark count (false click). This is in the end, reduces the maximum transmission distance.

3.5 Amplifier

AD8009 amplifier is used in the amplifier stage which is an ultrahigh speed current feedback amplifier with a 5,500 V/μs slew rate that results in a rise time of 545 ps making it ideal as a pulse amplifier and ideal for our pulse detection experiment. Data sheet for the AD8009 is given in Appendix C.

Amplifier Stage circuitry is designed using the evaluation board schematics of the amplifier. Gain of the circuitry shown in Figure 21 is calculated by the following formula;

$$G = 1 + \frac{R_1}{R_2} \tag{3.17}$$

Using the above formula, R_1 and R_2 resistor values are adjusted so that gain is equal to 10 (G=10).

C_1 and C_2 shunt capacitors are used for supply bypassing.

Figure 21 is simulated using the Capture Orcad Pspice program and the frequency response curve shown in

Figure **22** is obtained where the operational frequency range is approximately 100 MHz.

Same frequency response is evaluated experimentally by changing the frequency and observing the output voltage. Experiment results also confirm the simulation results.

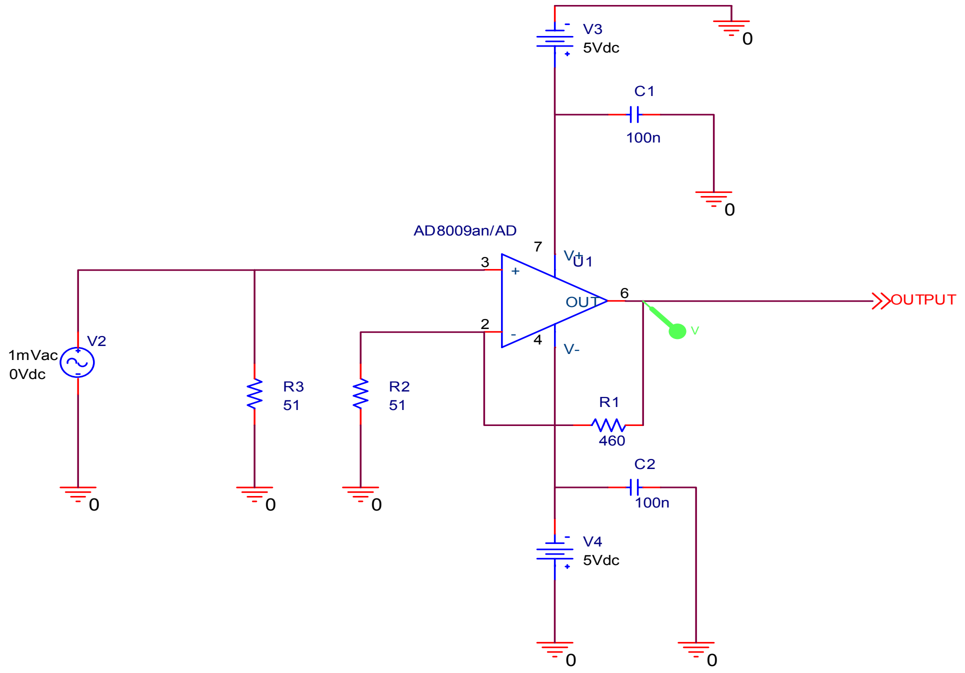

Figure 21 Amplifier circuitry

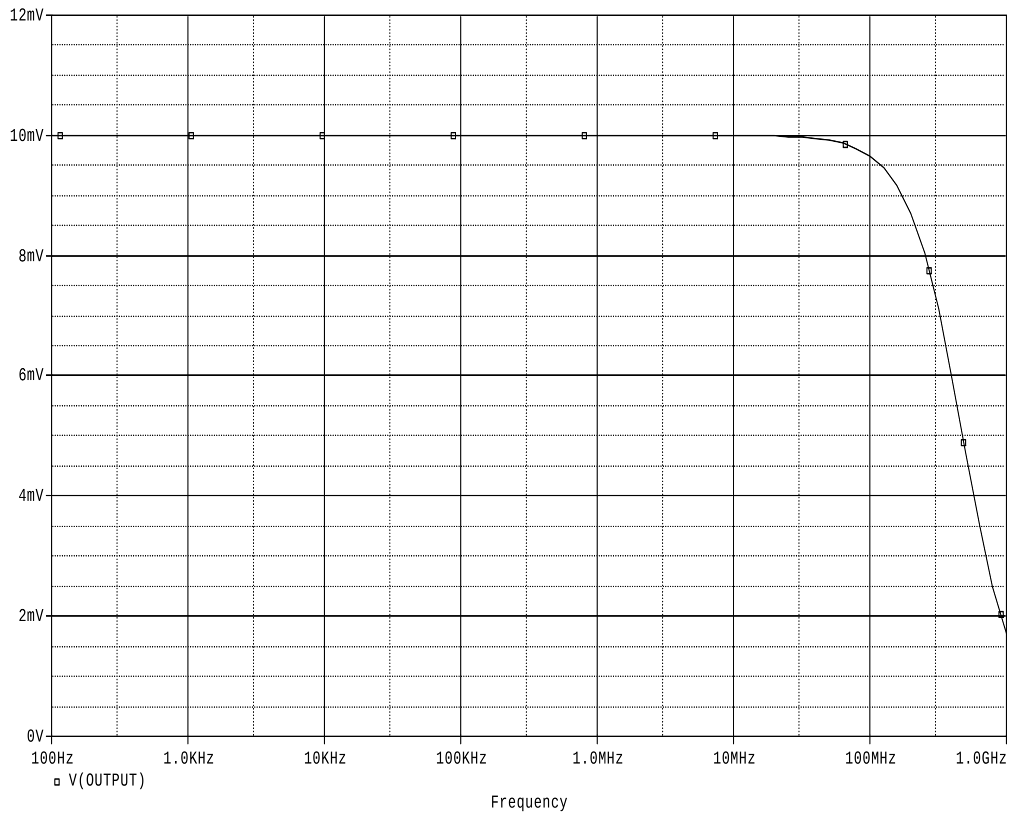

Figure 22 Frequency response of amplifier circuitry

PCB of amplifier circuitry is given in Figure 24. Right-angled SMA connectors are used for the signal input and output connection of the circuitry to the measurement equipment.

In order to evaluate the APD, a set of performance measures must be developed. This must be done to identify the optimal characteristics of operation because there is not an obvious way to find this. It is composed of several trade-offs.

3.6 Detection Circuitry

The basic configuration of the circuits around the APD as named detector in the experimental setup is shown in the Figure 23. This constitutes the Geiger mode configuration. When we anticipate an arrival of photon, the voltage is risen above the breakdown threshold. Normally no avalanche occurs, but if a photon actually comes in and is absorbed in the APD junction where it generates an electron-hole pair, this can cause an avalanche. The current through the APD quickly rises to macroscopic values (e.g. 0.5 mA) and we can observe a pulse at the output of the amplifier. When the voltage on the APD is lowered below the breakdown, the avalanche and the output pulse ends.

In the Figure 23, there is the pulse generator, then the transmission line is split into two by the delta coupler. This provides matching of impedance in all directions. The probe doesn’t contribute to any significant mismatch.

The APD circuitry has a high degree of symmetry. The gate pulses cause transients at its edges because of the junction capacitance of the APD. These transients are often higher in amplitude than the actual signal. Detection of a signal is therefore difficult since a transient is present at every gate and the avalanche is not. A differential circuit is used to cancel current spikes flowing through the APD capacitance at the rising and falling edges of the gating pulse. When it is properly tuned, i.e. when the length of transmission lines and the variable capacitor are adjusted to make the arms electrically identical in the absence of avalanches, there is no signal on the output. If an avalanche occurs, it produces a nice short pulse. By simulating the junction of the APD by using a capacitor $C = C_{APD} = 1.5$ pF which is equal to junction capacitance of the APD we used, the transients can be subtracted, leaving a somewhat clean signal. So, the two transmission lines are both terminated in a differential amplifier stage for transient subtraction.

Inside the APD package there are soldered terminations of transmission lines. Two 51 ohm resistors behind the APD and C reduce noise (ringing).

As in the amplifier stage, also in the differential stage AD8009 amplifier is used. The most important property that the differential stage should have is the capability of fast responding to very small signals which are in the order of milivolts.

Photograph of the printed circuit board of the detection circuitry is given in Figure 25 and Figure 26 shows its connections.

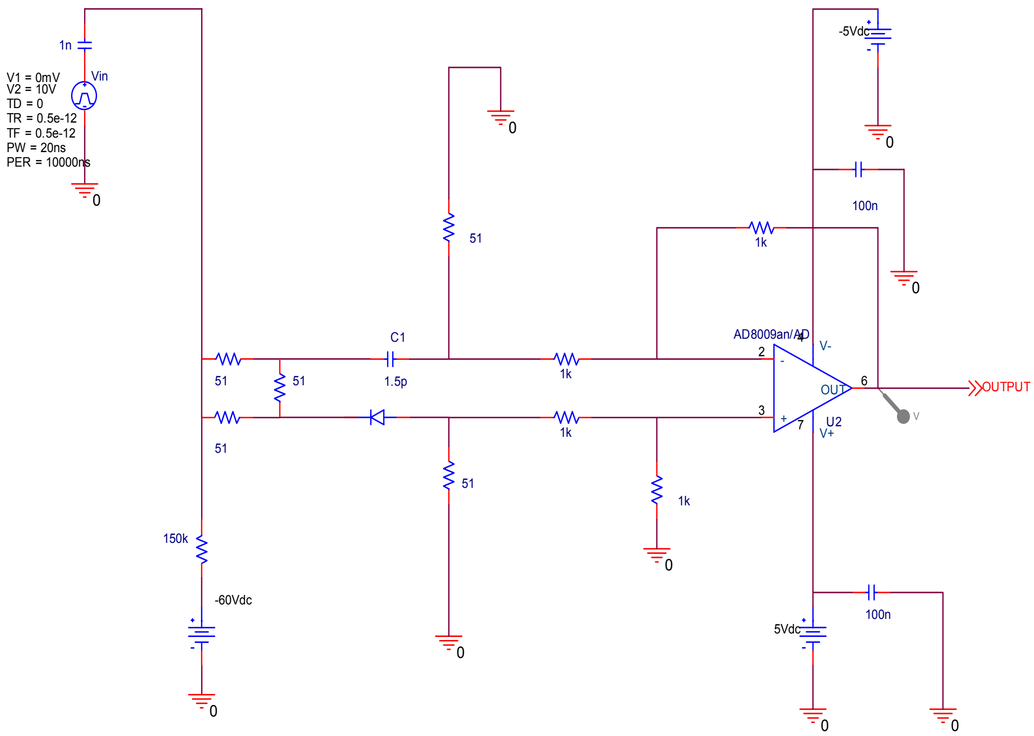

Figure 23 Detection circuitry

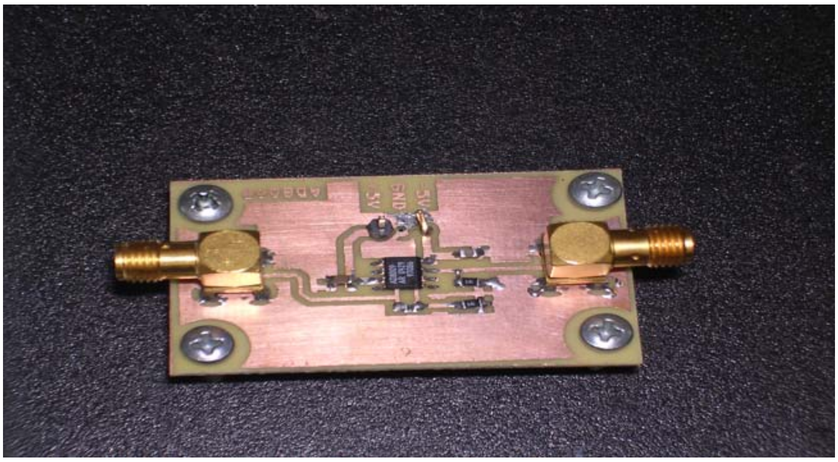

Figure 24 Amplifier

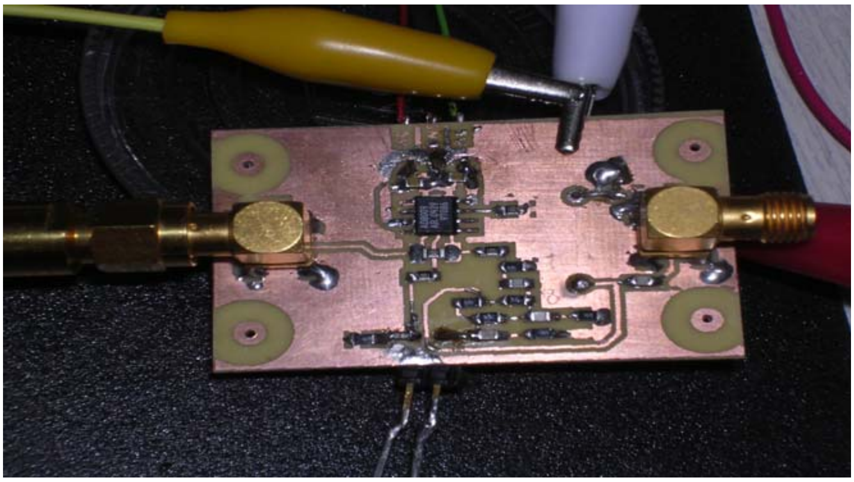

Figure 25 PCB of detection circuitry

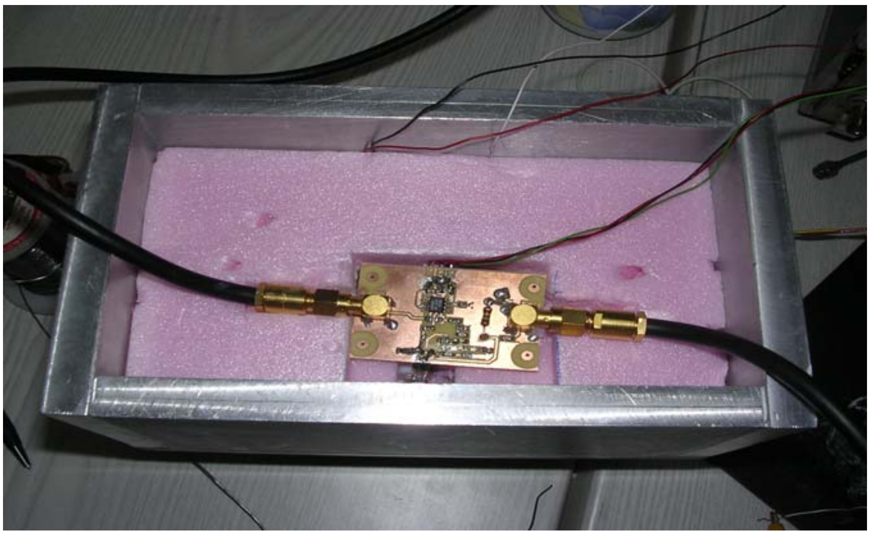

Figure 26 Connections of detection circuitry

3.6.1 Simulation of Detection Circuitry

The detection circuitry in Figure 31 is simulated in the Orcad p-spice program where APD is modeled as a diode and -60 V DC source and the results in Figure 27 are obtained.

It is a weak point that not to be able to model the EG&G APD. So the simulation results just pave way to estimate the response of the circuit.

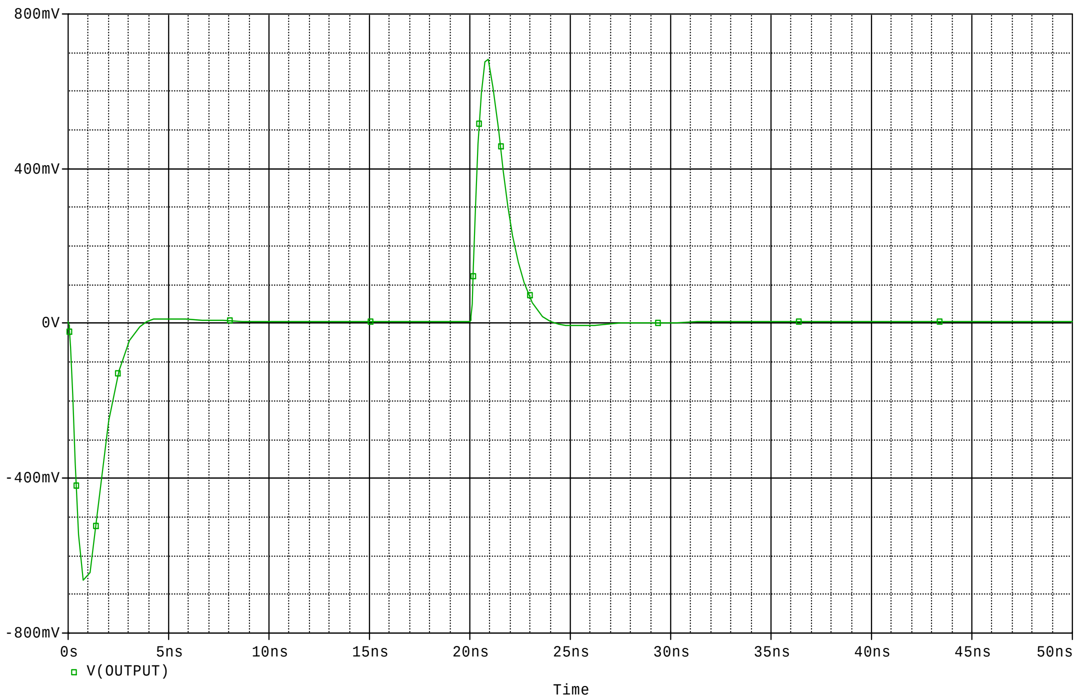

Figure 27 Simulation results

3.6.2 Preliminary Measurements

Before using the APD in the circuitry, a pulse source connected in parallel with a 100 KΩ resistor is used in place of the APD. Experiments results are given in Figure 28, Figure 29 and Figure 30. Experiment results show that for the increased values of gate width of the applied voltage source, smaller values of output is obtained. Since the voltage source doesn't conform with the operation of APD exactly, results are just useful to test the response of APD circuitry.

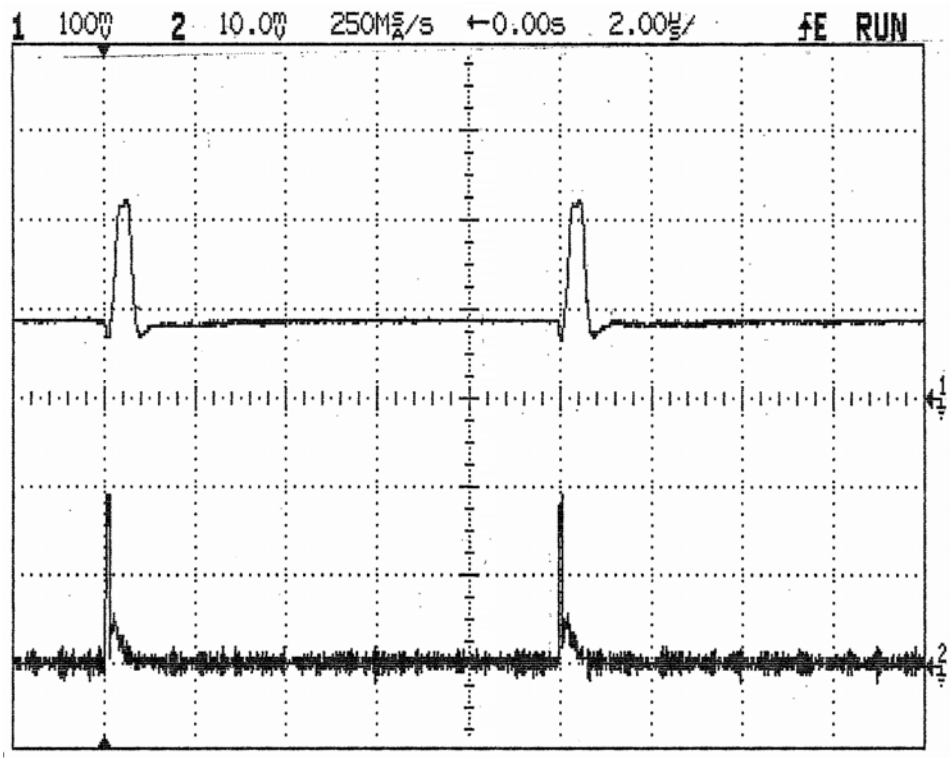

Figure 28 Preliminary measurement results for tg=100ns

Channel 1: Input pulse signal, Channel 2: APD Circuitry Output, V_{output} = 155 mVp.

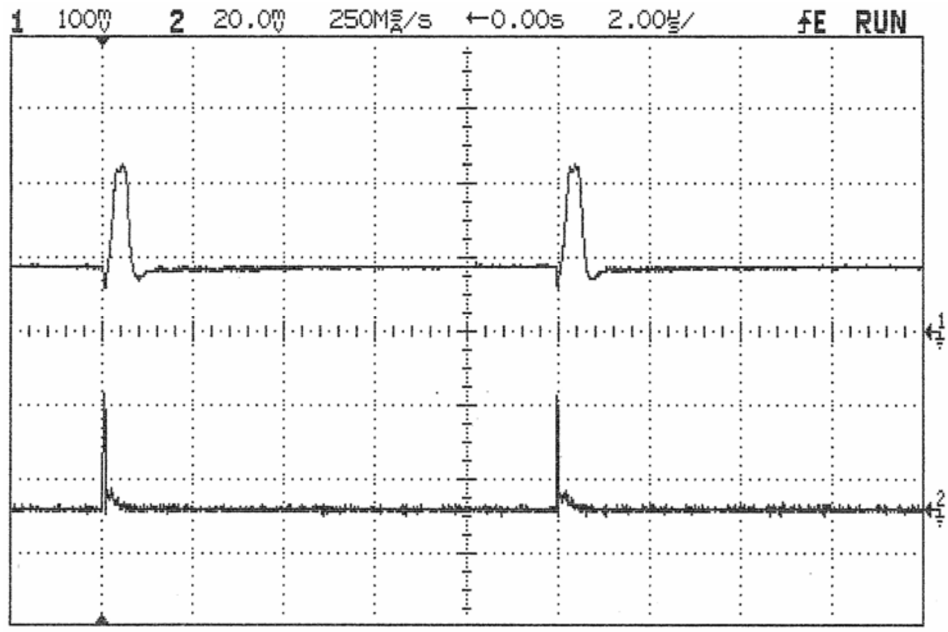

Figure 29 Preliminary measurement results for tg=50ns

Channel 1: Input pulse signal, Channel 2: APD Circuitry Output, V_{output} = 265 mVp.

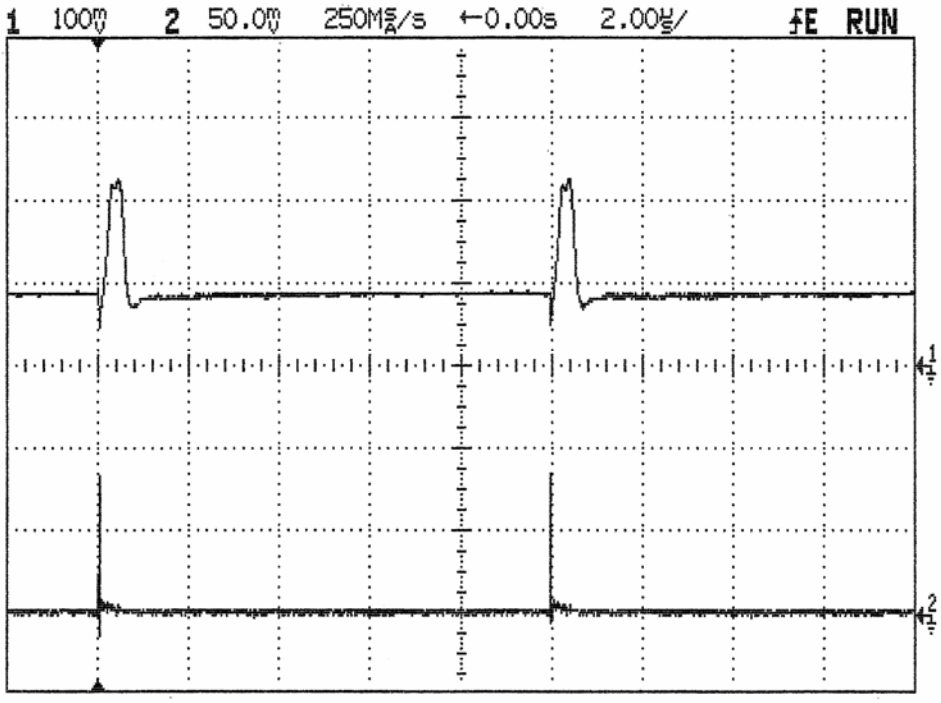

Figure 30 Preliminary measurement results for tg=20ns

Channel 1: Input pulse signal, Channel 2: APD Circuitry Output, V_{output} = 675 mVp.

3.7 Measures for the Performance of the APD

Many of the physical properties of the APD are related. Changing one property may often change others as well. To achieve the best possible performance all the operational parameters must be correctly set. However trying to improve one specific property by adjusting one parameter might not have the desired advantage. An improvement like this often causes a depreciation that cancels the achieved advantage. An example of this can be the Quantum Efficiency (QE) / dark count matter. Both properties increase when changing the excess voltage. This means that more photons can be detected successfully. But the dark current is subject to same the increased probability of detection. If both properties increase at the same rate no improvement is achieved, the ratio of photo count and dark count rate stays constant. It is though difficult to know in which order two competing properties change. If the good property improves for times and the bad depreciate twice it is safe to say that the adjustment was advantageous.

A set of performance measures, referred to as efficiencies, will bring the matter of all the competing properties into consideration. The efficiencies are concerning the three major properties:

- Dark counts,
- Photon detection,
- Repetition rate.

The two first are functions of X є {V_E, V_R, t_g} and f_{rep}. The upper boundary of a (dark/photo) count is the repetition rate.

The repetition rate is the maximal number of gates per second and a count is possible only when the APD is gated. The efficiencies are thought to reflect the portion of disadvantageous/advantageous instances to the replication rate. The efficiencies $\eta \rightarrow 1$ when subject to optimal conditions.

The object of this section is to establish a more general way of how to evaluate and APD as a single photon detector.

3.7.1 Dark Counts

Dark current counts are possible to measure by simply not coupling light into the fiber. Then for certain values of X and f_{rep} a dark count rate η_{dark} can be detected. The error rate in percent is

$$e(X,\mathrm{frep}) = \frac{\eta\,\mathrm{dark}}{\mathrm{frep}}.100\% \tag{3.18}$$

Assuming that a dark count corrupts the information and thereby makes it useless, leaves a portion of still potential useful bits.

In order to conduct a complete QC experiment the dark counts must be kept low. Otherwise, the error correction codes will not be able to do their jobs. A qualified guess dark count error rate is $e(X,\mathrm{frep})$ = 0.005.

Saying that a dark count makes the bit information useless is somewhat false. The instance where both a photon and dark current carrier is present at a gate might very well happen. Another instance is when the photon doesn't reach the APD and dark current carrier causes avalanche. In both examples the information is valid. For now this is a good model since it is desirable to keep the dark counts as low as possible.

3.7.2 Photon Detection

A problem arises when single photon is to be counted. There is no way to avoid dark counts which will as well as the photo counts, contribute to the total number of counts. Also, the laser light source can not deterministically emit only one photon per pulse. The number of photons in a pulse is described by statistics, making it even a little more complicated.

The laser can have photon (pulse) efficiency η_{photon} =0.5 meaning 5 photons per 10 pulses. The rate of photons sent is

$$\eta_{sent} = \eta_{photon} \cdot f_{rep} \tag{3.19}$$

Since the detector is supposed to detect single photons the photon efficiency of the laser must be kept > 1. If not, there is a too high probability that more than one photon is emitted in a pulse. This in term makes it impossible to determine the exactly when a photon arrives. The efficiency of detection must therefore be based on the differential figure of detected counts and dark counts. The rate of dark counts η_{dark} must be determined in under identical conditions as for the detection trial since there is less that one photon per pulse the rate of detected photons is given by

$$\eta_{\text{photons}} = \frac{\eta_{detected}}{\eta_{photon}} - \eta_{dark} \tag{3.20}$$

$$= \frac{\eta_{detected} - \eta_{photon} \cdot \eta_{dark}}{\eta_{photon}}$$

The rate of photons detected are related to the replication rate

$$\eta_{\text{photons}}(X, f_{rep}) = \frac{\eta_{photons}}{f_{rep}} \tag{3.21}$$

$$= \frac{\frac{\eta_{detected} - \eta_{photon} . \eta_{dark}}{\eta_{photon}}}{f_{rep}}$$

$$= \frac{\eta_{detected} - \eta_{photon} . \eta_{dark}}{\eta_{photon} \cdot f_{rep}}$$

The photons will then, if detected, cause $\eta_{detected} > \eta_{dark}$. The magnitude of $\eta_{detected}$ tells how many of the counts that actually are correct.

The theoretical figure of detector efficiency is embedded into the expression. The detector efficiency is given by

$$\eta_{detected} = \eta_{QE} . \text{(connectors)}. \text{(fiber)} \tag{3.22}$$

$$= \eta_{QE} . d_{connector} . d_{fiber}$$

η_{QE} is therefore slightly large that what measured.

3.7.3 Repetition Rate

Increasing the repetition rate might increase the dark counts, but at the same time more bits are successfully transferred.

When the gate is off there is some dead time t_{off} where photons can not be detected nor sent. This off time is useless in the sense of transmission. The maximum value of f_{rep} is in experiments like these about f_{max} = 1 MHz.

We have that

$$\frac{1}{f_{rep}} = t_g + t_{off} \tag{3.23}$$

Since $t_g << t_{off} \Rightarrow t_{off} = \frac{1}{f_{max}}$, the measure of utilization of time can therefore be written

$$\eta_{rep}(f_{rep}) = \frac{f_{rep}}{f_{max}} \tag{3.24}$$

Low repetition rate f_{rep} utilizes the time poorly. While when $f_{rep} = f_{max}$ the APD is used at its maximum limit. This limit can be set by a high number of dark counts. To compare several APDs the f_{max} must be set to a fixed value for all trails. Unless this is done it will be impossible to evaluate the processes data.

The repetition rate problems can be made insignificant by applying an adaptive repetition rate circuitry. Its only when an avalanche has occurred that the APD needs rest due to carrier trapping. Theoretically, in absence of avalanches, the APD can be gated at a rate of magnitude of tens of MHz. This will not be dealt with in this thesis.

3.7.4 Affects of measures to the performance

Physical and operational properties of the APD has several effects on the performance of the APD. These are explained as follows.

3.7.4.1 Excess Voltage, V_E

The excess bias has two apparent effects; increases both detector efficiency and dark current counts.

The excess bias V_E is proportionally related to the e-field inside the APD. This in term decides the magnitude of the ionization coefficients. When raising the V_E it is therefore expected that probability of an avalanche is increased. That is when a photo generated carrier is present. V_E is therefore preferred as high as possible in order achieve the best quantum efficiency for the APD as possible.

V_E is expected to increase dark current counts. It will not alter the rate of thermally generated carriers. By increasing the V_E the ionization coefficients increases and thereby also the dark current counts. These carriers are subject to the same increased probabilities for avalanche as the photo generated ones.

3.7.4.2 Bias Voltage, V_R

V_R sets the magnitude of e-field when gate is off. It is therefore the parameter that sets the operational characteristic when the APD is off.

The bias V_R must be operated below breakdown V_B. Above V_B the dark current will multiply. A saturated current will continuously flow through the APD according to magnitude of the bias.

The bias will have a reducing effect on some of the dark counts. Trapped holes in the heterobarrier is during gate off time swept out of the junction. The extent of this sweeping is somewhat fussy but it is expected that a highest possible V_R right below V_B will sweep the most holes. This is because the largest V_R gives the strongest e-field.

3.7.4.3 Gate Width, tg

A number of carriers are passing a cross section of the APD due to dark current. The probability of a carrier being present within the gated period D is proportionally increased by a large t_g. This increases probability of an avalanche and thereby a dark current count. Equally, the dark current counts will decrease when t_g is reduced.

Trapping occurs when carriers passes the junction. The magnitude of the charge passing a cross section of the junction is given by the length of the gate. An avalanche is only possible during a gate pulse. The avalanche will also last until gate is off. A short gate length will reduce the probability of some trapped charge. The less charge in the barrier the less probability of dark count at the next gate pulse.

An interesting combination is between V_E and t_g. To compensate for increased dark current counts when increasing the excess voltage the gate width can be reduced. The overall result is better detector efficiency at a constant dark current count level.

CHAPTER 4

MEASUREMENTS

In this chapter, the equipment used in the experimental setup shown in Figure 4 and measurement results of the experiment will be given.

4.1 Equipment Used

A photograph of the established experimental setup is shown in Figure 31. Equipment used in the experimental setup is as follows:

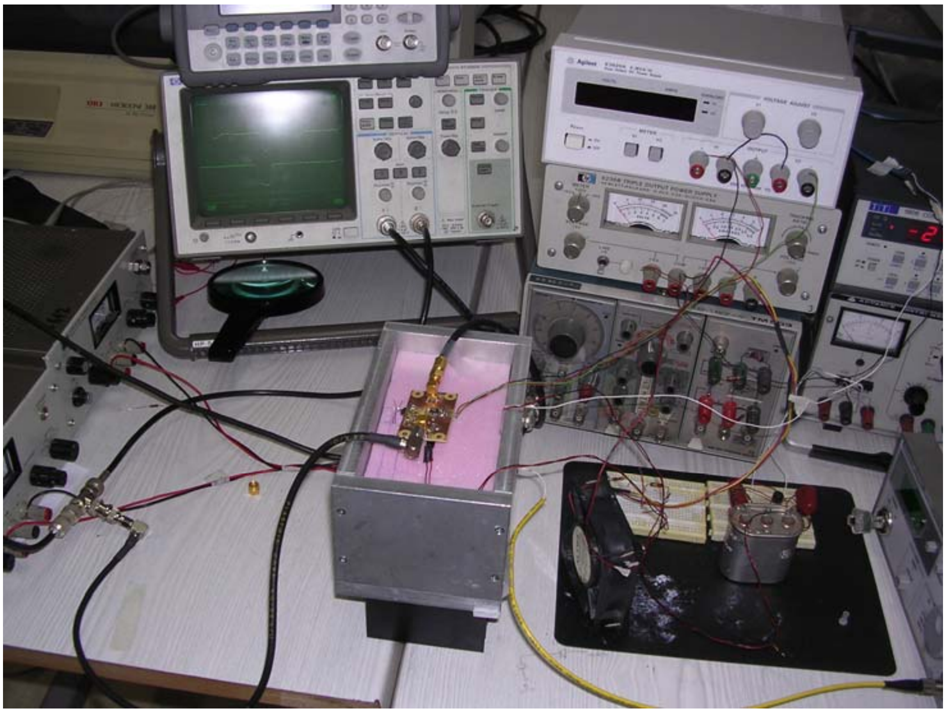

Figure 31 Experimental setup

LASER: Lasetron QLM 55876 is used in the experiment as the optical signal source. Controller of the LASER is AD 9661. Laser has a TTL output for modulation and a bandwidth of 128 Mb/s.

ATTENUATOR: HP 8156 is used to attenuate the pulses received from the LASER.

SCOPE: HP 54616 is used to monitor output of the experimental setup.

COMPUTING MULTIMETER: TT Instruments 1906 is a digital multimeter that the temperature of the APD assembly is easily measured by connecting the temperature control and measurement integrated circuit to the multimeter.

PULSE GENERATOR: Tektronix TM503 is a high voltage pulse generator used to supply pulses for the APD and the Laser.

4.2 Measurement Results

4.2.1 Gated Mode Response

In this case, pulse input is applied to the circuitry and response of the circuitry is monitored at the ambient temperature. No optical signal is applied. Measurement results are as shown in Figure 32, where

Vg = 10 Vp-p
tg = 200 ns
Vr = 50 V
Output = 150 mVp

Channel 1 shows the output, Channel 2 shows the input gate signal and lower plots show the details of the selected regions of the upper plots.

At the edge of the output pulse, ripples can be seen indicating the avalanche operation of the APD.

4.2.2 Ambient Temperature Response

In this case, optical input is applied to the circuitry and response of the circuitry is monitored at the ambient temperature. Measurement results are as shown in Figure 33, where

Temperature = 24°C
Optical input = 0.6 mW
Vr = 43 V
Output = 2 mVp-p

The output has a low dark count rate for the above conditions.

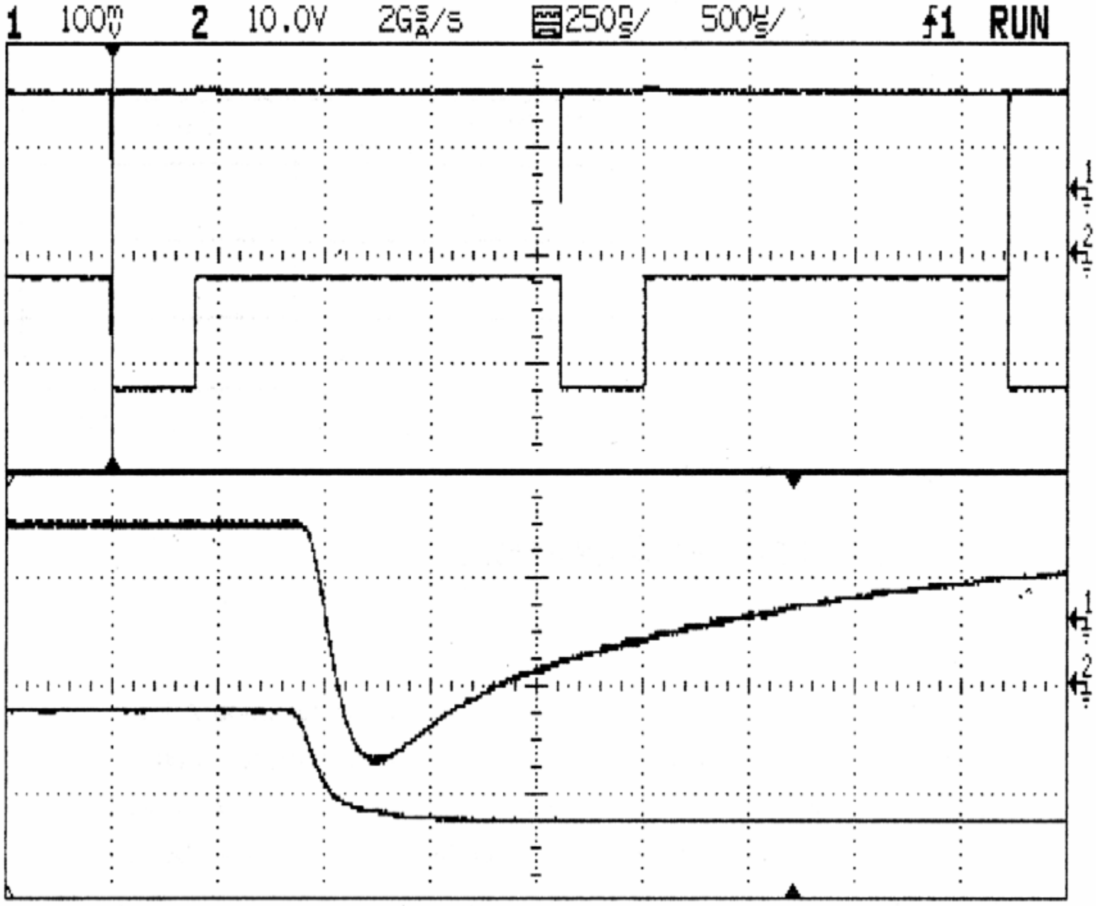

Figure 32 Gated mode response

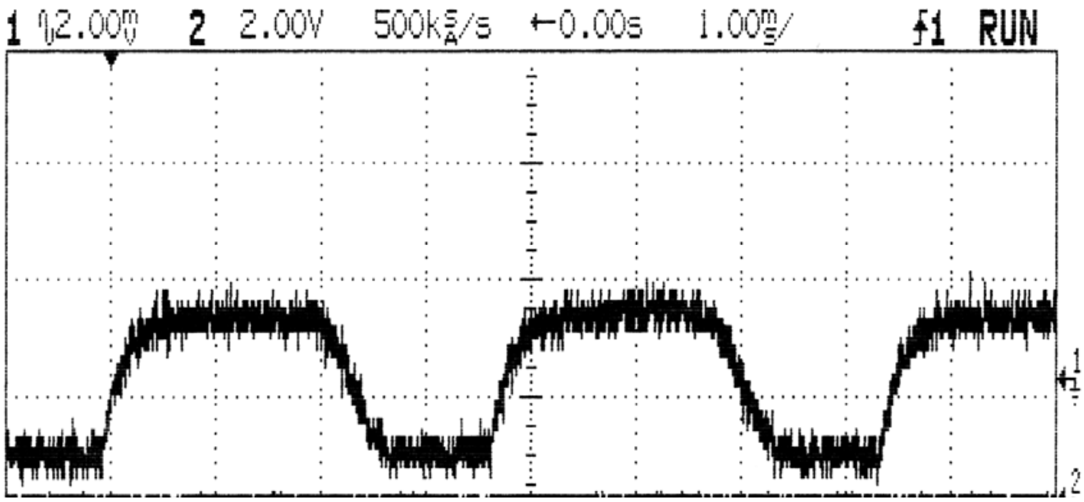

Figure 33 Ambient temperature response

4.2.3 Low Temperature Response

In this case, optical input is applied to the circuitry and response of the circuitry is monitored at the minimum temperature reached using TECs. Measurement results are as shown in Figure 34, where

Temperature = - 25°C

Optical input = 0.6 mW

Vr = 43 V

Output = 2 mVp-p

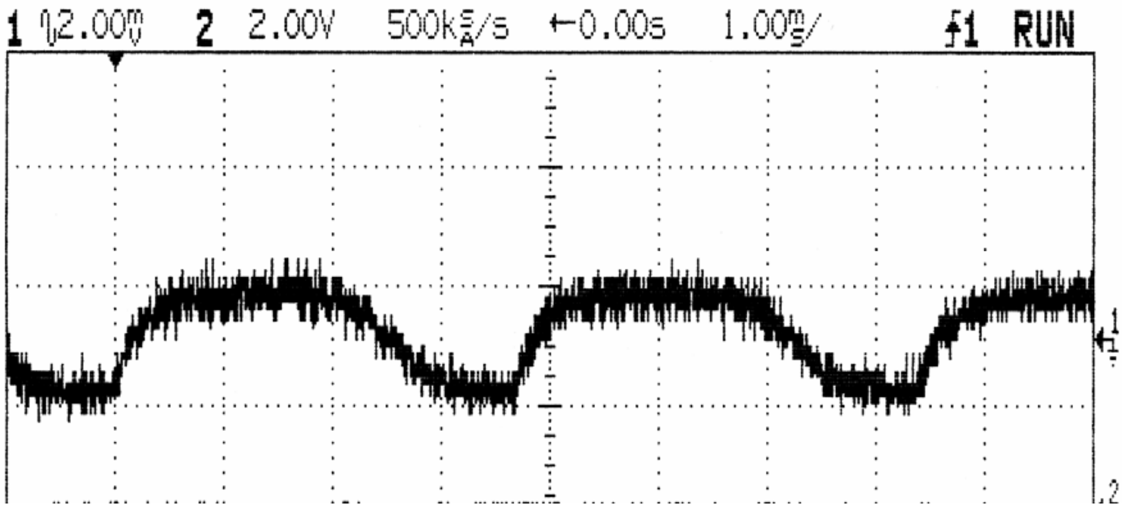

Figure 34 Low temperature response

As it is seen from the Figure 34, minimum reached temperature is insufficient to decrease the dark count rate since the decrease of temperature didn't change the output dark current rate and still dark count rate is not sufficiently small.

CHAPTER 5

CONCLUSIONS

The experimental studies have shown that construction of a single photon detection receiver is rather difficult and there are many critical issues to be considered. The experimental setup assembled for the present work has demonstrated that an APD such as EG&G 30644 is the correct choice as a low noise device. However; the packaging is TO-18 case with an optical window. The details required in mounting and optically matching the fiber to APD has been difficult to solve. Hence; an APD with a pig tail construction could have simplified the mechanical assembly.

The temperatures obtained during cooling represents a condition where there is a very low dark noise. However; it is estimated that dark current noise is still high at present operating temperatures. Either an improved thermoelectrical cooling or an entirely different cooling such as liquid nitrogen cooling is needed in future studies. The quenching circuit used seems to be satisfactory and efficiently quenches the APD. It is our conclusion that passive quenching is sufficient in high speed operation of APD.

The preamplifier circuit which is based on AD8009 is a simple and reliable circuit. Although it has a low gain, which needs further amplification, it enables detection of low level currents. The disadvantage of the circuit used stems from the compensating capacitance used, which has to be matched to APD capacitance. It was observed that this capacitance should be adjustable to provide matching in circuit.

Simulation results confirmed the experimental results as far as bandwidth and rise times of AD8009 based circuit. Although p-spice model for AD8009 was available; no such model could be found for EG&G 30644 APD. This was a weak point in simulations.

As future study, it is suggested to try a liquid nitrogen cooling or much improved thermoelectrically cooling assemblies for low noise operation of EG&G 30644 APD.

REFERENCES

[1] Bennett, C. and Gilles, B., *Quantum Cryptography: Public Key Distribution and coin Tossing*, International Conference on Computers, Systems and Signal possessing, Bangalore, India, 1984

[2] Wiesner, S., *SIGACT News* 15, 78 (1983); C. H. Bennett, *Science* 257, 752 (1992)

[3] Hughes, R., *Quantum Cryptography over underground optical fibers,* Advances in Cryptology, Volume 1109, August 1996, pp. 329-342

[4] Hughes, R., Nordholt, J., Derkacs, D. and Peterson, C., *Practical free-space quantum key distribution over 10 km in daylight and at night*, New J. Physics, July 2002, pp. 43

[5] Rarity, J., Tapster, P., Gorman, P., and Knight, P., *Ground to satellite secure key Exchange using quantum cryptography*, New J. Physics, October 2002, Volume 4, pp. 82

[6] Ribory, G., Brendel, J., Gautier, J.D., Gisin, N., and Zbinden, H., *Long distance entanglement based quantum key distribution*, Physics Rev. A V. 63, December 2000

[7] Nambu, Y. and Kosaka, H., *Introduction of Quantum Cryptography and Its Development*, NEC Res. and Develop., Vol 44, No. 3, July 2003, pp. 1

[8] Chip, E., David P., Gregory T., *Quantum Cryptography in Practice*, May 2003

[9] Gisin, N., Ribordy, G., Tittel, W., and Zbinden, H., *Quantum Cryptography*, Reviews of Modern Physics, Volume 74, 8 March 2002, pp. 155-156

[10] Torbjoern, N., *Single Photon Detection using Avalanche Photodiode*, January 1999

[11] Refaat, T.F., Luck, W.S., Deyoung, R. J., *Temperature Control of Avalanche Photodiode Using Thermoelectric Cooler*, October 1999, pp. 1-6

[12] Lucien, H., *Interferometers for long-distance quantum key distribution*, 2002, pp. 3

[13] Bethune, D. and Risk, W., *Autocompensating quantum cryptograph*y, New J. Physics, Volume 4, July 2002, pp.42

[14] Stucki, D., Gisin, N., Guinnard, O., Ribordy, G. and Zbinden, H., *Quantum key distribution over 67 km with a plug&play system*, New J. Phys., July 2002, pp.41

APPENDIX A

APD DATA SHEET

In this appendix the data sheet of the EG&G APD used in the experiments is given.

EG&G®

InGaAs Avalanche Photodiode

C30733E/C30644E/C30645E

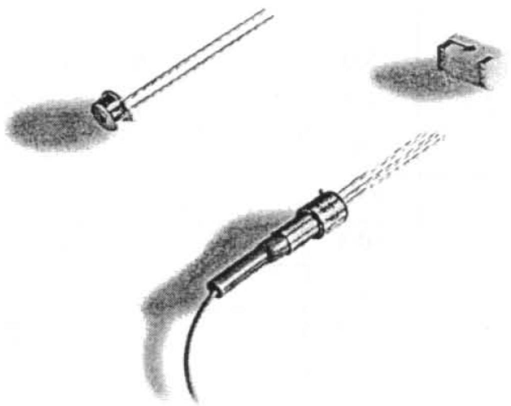

Description

EG&G's C30644, C30645 and C30733 serie high speed InGaAs/InP avalanche photodiodes. Their structure provides fast response and high quantum efficiency in the spectral range between approximately 1100nm and 1700nm. The APDs are optimized for use in fiber-optic communication systems, OTDRs, and range finders with 1300 to 1550nm wavelength ranges The photodiodes are available on a ceramic carrier for use in hybrid applications. The C30644 and C30645 are also offered in the D2, D11 and D12 outlines.

Quality & Reliability

EG&G Optoelectronics Canada is committed to supplying the highest quality product to our customer. We are certified to meet ISO-9001 and are designed to meet Bellcore quality specification TA-NWT-00983. All devices undergo extended burn-in and periodic process qualification programs to assure high reliability.

Features

- Spectral response (1100 to 1700nm)
- High responsivity
- Bandwidth to 2.5 GHz
- Low dark current and noise

Applications

- OC-12, OC-48 receiver modules
- OTDR
- Range finding

Specifications (at M = 10 @ 25)

PARAMETER	C30733			C30644			C30645			UNITS
	MIN	TYP	MAX	MIN	TYP	MAX	MIN	TYP	MAX	
Active Diameter		30			50			80		µm
Breakdown Voltage		60			60			60		Volts
Gain[3] (M)		10			10			10		
Temperature coefficient of V_r for constant gain		0.15			0.20			0.20		V/°C
Quantum Efficiency[3]										
1300nm		85		75	85			85		%
1550nm		75		65	75			75		%
Responsivity										
1300nm	7.9	8.9		7.9	8.9		7.9	8.9		A/W
1550nm	8.1	9.4		8.1	9.4		8.1	9.4		A/W
Total Dark Current (M = 10)		<1			5	10		10	25	nA
K_{eff}		0.45			0.45	0.55		0.45		
Noise Current (M = 10)		<0.1			0.15	0.25		0.25	1.0	pA/Hz$^{1/2}$
Capacitance (M = 10) ECER		0.26			0.6	0.8		1.5		pF
Frequency Response (3db) M = 10		3000			2000			1000		MHz

NOTES:

1. A specific voltage, V, is supplied with each device. When the photodiode is operated at this voltage (at 23°C), the device will meet the electrical characteristic limits shown above. The voltage value will be within the range of 40 to 90 volts.

2. The voltage dependence of the gain, for gains above about 4, is given approximately by the following empirical formula: $M = 50 / (V_b - V)$.

3. Gain and quantum efficiency are not directly measurable quantities. The numbers quoted are estimated typical values. Gain, quantum efficiency and responsivity are related by the following: $R = \eta\lambda M / 1.24$ where λ is the wavelength in units of µm, η is the quantum efficiency, M is gain.

4. The detector noise current / Hz$^{1/2}$ is given by the following expression:

   $$in = (2q\,(Is + IbM^2 F))^{1/2}$$

   where: $F = k_{eff}M + (1-k_{eff})(2-1/M)$ and I_s and I_b are the unmultiplied and multiplied portions of the dark current, respectively. The total dark current is given by: $It = I_s + I_b M$.

   However, since both I_s and I_b are somewhat voltage dependent, and M is not directly measurable (see Note 3), it is not usually possible to determine both I_s and I_b unambiguously. Since system performance depends on noise current and responsivity, these measurable quantities are the ones which have been specified.

5. Most devices can be operated at gains up to about 30 or more, but with values of noise current correspondingly higher, as indicated by the discussion in Note 4 above.

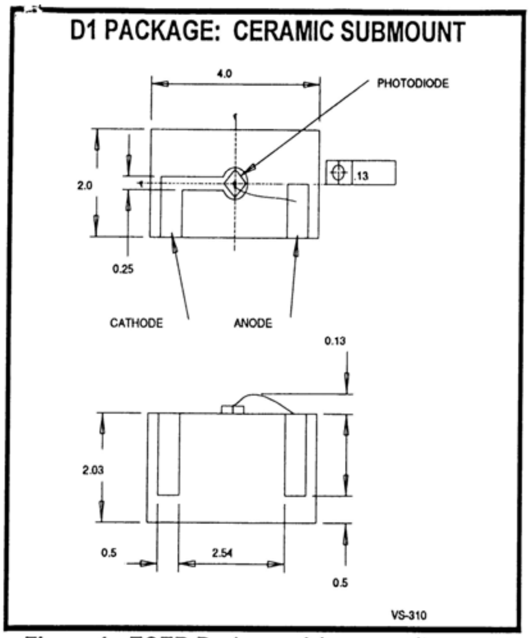

Figure 1: ECER Package: A low capacitance ceramic block for hybrid assemblies.

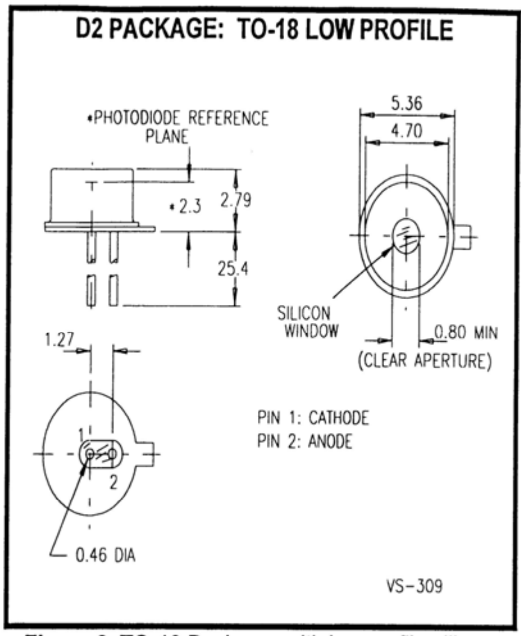

Figure 2 TO-18 Package, with low-profile silicon window cap for reduced window-chip distance. Available only for the C30644.

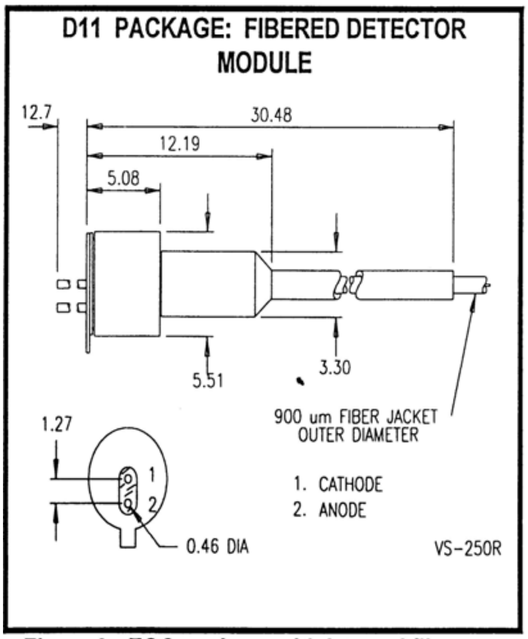

Figure 3: EQC package with integral fiber optic pigtail. Available only for the C30644.

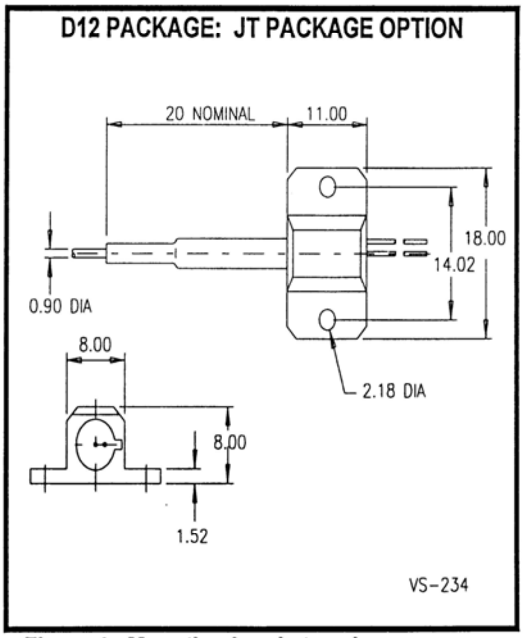

Figure 4: Mounting bracket package. Available only for the C30644.

Absolute Maximum Ratings, Forward Current, I_F:

Standard TO-18 Package	5mA
Ceramic Package	5mA
Pigtailed Package	5mA

Total Power Dissipation, PT:

Standard TO-18 Package	20mW
Ceramic Package	20mW
Pigtailed Package	20mW

Ambient Temp/Storage:

Standard TO-18 package	-60 to +125°C
Ceramic Package	-60 to +125°C
Pigtailed Package	-60 to +125°C
Operating TA:	
Standard TO-18 package	-20 to +70°C
Ceramic Package	-20 to +70°C
Pigtailed Package	-20 to +70°C
Soldering (10S) Tsd:	
Standard TO-18 package	250°C
Ceramic Package	250°C
Pigtailed Package	250°C

Typical Spectral Responsivity vs Wavelength (nm), Gain = 10, Temp. = 20°C

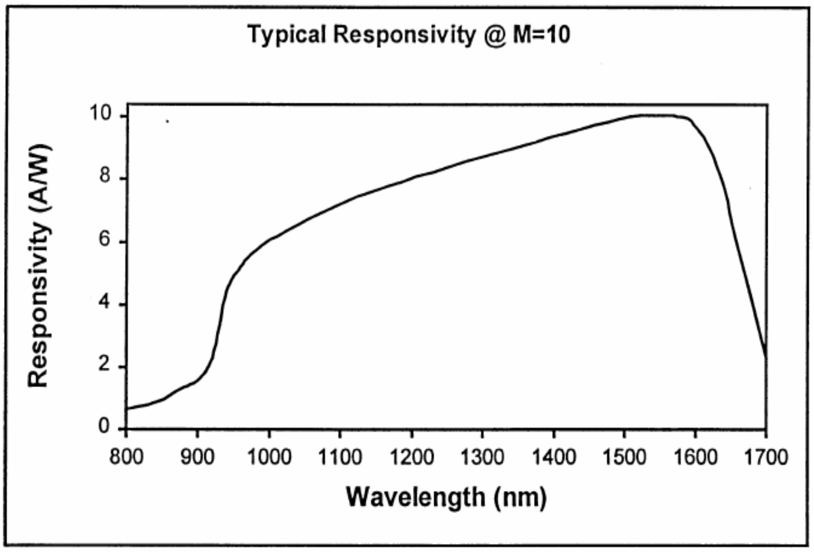

APPENDIX B

TEMPARATURE CONTROL and MEASUREMENT INTEGRATED CIRCUIT DATA SHEET

In this appendix, selected pages of the data sheet of the TMP01 temperature control and measurement integrated circuit is given.

ANALOG DEVICES

Low Power, Programmable Temperature Controller

TMP01*

FEATURES
- –55°C to +125°C (–67°F to +257°F) Operation
- ±1.0°C Accuracy Over Temperature (typ)
- Temperature-Proportional Voltage Output
- User Programmable Temperature Trip Points
- User Programmable Hysteresis
- 20 mA Open Collector Trip Point Outputs
- TTL/CMOS Compatible
- Single-Supply Operation (4.5 V to 13.2 V)
- Low Cost 8-Pin DIP and SO Packages

APPLICATIONS
- Over/Under Temperature Sensor and Alarm
- Board Level Temperature Sensing
- Temperature Controllers
- Electronic Thermostats
- Thermal Protection
- HVAC Systems
- Industrial Process Control
- Remote Sensors

FUNCTIONAL BLOCK DIAGRAM

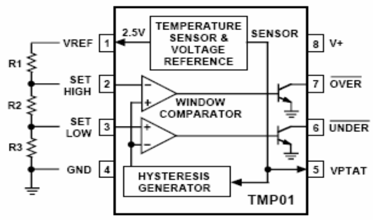

GENERAL DESCRIPTION

The TMP01 is a temperature sensor which generates a voltage output proportional to absolute temperature and a control signal from one of two outputs when the device is either above or below a specific temperature range. Both the high/low temperature trip points and hysteresis (overshoot) band are determined by user-selected external resistors. For high volume production, these resistors are available on-board.

The TMP01 consists of a bandgap voltage reference combined with a pair of matched comparators. The reference provides both a constant 2.5 V output and a voltage proportional to absolute temperature (VPTAT) which has a precise temperature coefficient of 5 mV/K and is 1.49 V (nominal) at +25°C. The comparators compare VPTAT with the externally set temperature trip points and generate an open-collector output signal when one of their respective thresholds has been exceeded.

Hysteresis is also programmed by the external resistor chain and is determined by the total current drawn out of the 2.5 V reference. This current is mirrored and used to generate a hysteresis offset voltage of the appropriate polarity after a comparator has been tripped. The comparators are connected in parallel, which guarantees that there is no hysteresis overlap and eliminates erratic transitions between adjacent trip zones.

The TMP01 utilizes proprietary thin-film resistors in conjunction with production laser trimming to maintain a temperature accuracy of ±1°C (typ) over the rated temperature range, with excellent linearity. The open-collector outputs are capable of sinking 20 mA, enabling the TMP01 to drive control relays directly. Operating from a +5 V supply, quiescent current is only 500 µA (max).

The TMP01 is available in the low cost 8-pin epoxy mini-DIP and SO (small outline) packages, and in die form.

*Protected by U.S. Patent No. 5,195,827.

REV. C

One Technology Way, P.O. Box 9106, Norwood. MA 02062-9106, U.S.A.
Tel: 617/329-4700 Fax: 617/326-8703

ABSOLUTE MAXIMUM RATINGS

Maximum Supply Voltage . . . . –0.3 V to +15 V
Maximum Input Voltage
(SETHIGH, SETLOW) . . . . –0.3 V to [(V+) +0.3 V]
Maximum Output Current (VREF, VPTAT) . . . . 2 mA
Maximum Output Current (Open Collector Outputs) . . 50 mA
Maximum Output Voltage (Open Collector Outputs) . . . . 15 V
Operating Temperature Range . . . . –55°C to +150°C
Dice Junction Temperature . . . . +150°C
Storage Temperature Range . . . . – 65°C to +150°C
Lead Temperature (Soldering, 60 sec) . . . . +300°C

Package Type	θ_{JA}	θ_{JC}	Units
8-Pin Plastic DIP (P)	103[1]	43	°C/W
8-Lead SOIC (S)	158[2]	43	°C/W
8-Lead TO-99 Can (J)	150[1]	18	°C/W

NOTES
[1] θ_{JA} is specified for device in socket (worst case conditions).
[2] θ_{JA} is specified for device mounted on PCB.

CAUTION

1. Stresses above those listed under "Absolute Maximum Ratings" may cause permanent damage to the device. This is a stress rating only and functional operation at or above this specification is not implied. Exposure to the above maximum rating conditions for extended periods may affect device reliability.
2. Digital inputs and outputs are protected, however, permanent damage may occur on unprotected units from high energy electrostatic fields. Keep units in conductive foam or packaging at all times until ready to use. Use proper antistatic handling procedures.
3. Remove power before inserting or removing units from their sockets.

ORDERING GUIDE

Model/Grade	Temperature Range[1]	Package Description	Package Option
TMP01EP	XIND	Plastic DIP	N-8
TMP01FP	XIND	Plastic DIP	N-8
TMP01ES	XIND	SOIC	SO-8
TMP01FS	XIND	SOIC	SO-8
TMP01FJ[2]	XIND	TO-99 Can	H-08A
TMP01GBC	+25°C	Die	

NOTES
[1] XIND = –40°C to +85°C.
[2] Consult factory for availability of MIL/883 version in TO-99 can.

GENERAL DESCRIPTION

The TMP01 is a very linear voltage-output temperature sensor, with a window comparator that can be programmed by the user to activate one of two open-collector outputs when a predetermined temperature setpoint voltage has been exceeded. A low drift voltage reference is available for setpoint programming.

The temperature sensor is basically a very accurately temperature compensated, bandgap-type voltage reference with a buffered output voltage proportional to absolute temperature (VPTAT), accurately trimmed to a scale factor of 5 mV/K. See the Applications Information following.

The low drift 2.5 V reference output VREF is easily divided externally with fixed resistors or potentiometers to accurately establish the programmed heat/cool setpoints, independent of temperature. Alternatively, the setpoint voltages can be supplied by other ground referenced voltage sources such as user-programmed DACs or controllers. The high and low setpoint voltages are compared to the temperature sensor voltage, thus creating a two-temperature thermostat function. In addition, the total output current of the reference (I_{VREF}) determines the magnitude of the temperature hysteresis band. The open collector outputs of the comparators can be used to control a wide variety of devices.

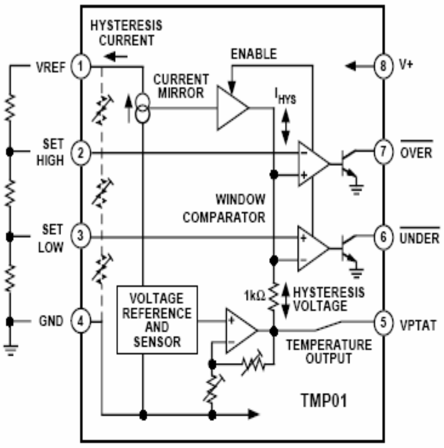

Figure 1. Detailed Block Diagram

Temperature Hysteresis

The temperature hysteresis is the number of degrees beyond the original setpoint temperature that must be sensed by the TMP01 before the setpoint comparator will be reset and the output disabled. Figure 2 shows the hysteresis profile. The hysteresis is programmed by the user by setting a specific load on the reference voltage output VREF. This output current I_{VREF} is also called the hysteresis current, which is mirrored internally and fed to a buffer with an analog switch.

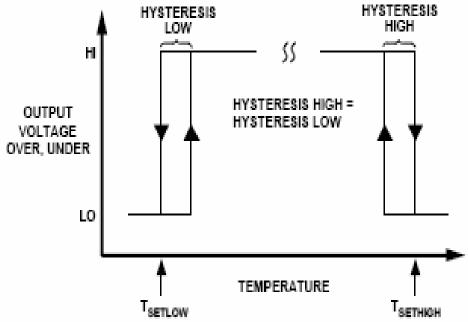

Figure 2. TMP01 Hysteresis Profile

After a temperature setpoint has been exceeded and a comparator tripped, the buffer output is enabled. The output is a current of the appropriate polarity which generates a hysteresis offset voltage across an internal 1000 Ω resistor at the comparator input. The comparator output remains "on" until the voltage at the comparator input, now equal to the temperature sensor voltage VPTAT summed with the hysteresis offset, has returned to the programmed setpoint voltage. The comparator then returns LOW, deactivating the open-collector output and disabling the hysteresis current buffer output. The scale factor for the programmed hysteresis current is:

$$I_{HYS} = I_{VREF} = 5\ \mu A/°C + 7\ \mu A$$

Thus since VREF = 2.5 V, with a reference load resistance of 357 kΩ or greater (output current 7 µA or less), the temperature setpoint hysteresis will be zero degrees. See the temperature programming discussion below. Larger values of load resistance will only decrease the output current below 7 µA and will have no effect on the operation of the device. The amount of hysteresis is determined by selecting a value of load resistance for VREF, as shown below.

Programming the TMP01

In the basic fixed-setpoint application utilizing a simple resistor ladder voltage divider, the desired temperature setpoints are programmed in the following sequence:

1. Select the desired hysteresis temperature.
2. Calculate the hysteresis current I_{VREF}.
3. Select the desired setpoint temperatures.
4. Calculate the individual resistor divider ladder values needed to develop the desired comparator setpoint voltages at SETHIGH and SETLOW.

The hysteresis current is readily calculated, as shown. For example, for 2 degrees of hysteresis, I_{VREF} = 17 µA. Next, the setpoint voltages $V_{SETHIGH}$ and V_{SETLOW} are determined using the VPTAT scale factor of 5 mV/K = 5 mV/(°C + 273.15), which is 1.49 V for +25°C. We then calculate the divider resistors, based on those setpoints. The equations used to calculate the resistors are:

$$V_{SETHIGH} = (T_{SETHIGH} + 273.15)(5\ mV/°C)$$

$$V_{SETLOW} = (T_{SETLOW} + 273.15)\ (5\ mV/°C)$$

$$R1\ (k\Omega) = (V_{VREF} - V_{SETHIGH})/I_{VREF} = (2.5\ V - V_{SETHIGH})/I_{VREF}$$

$$R2\ (k\Omega) = (V_{SETHIGH} - V_{SETLOW})/I_{VREF}$$

$$R3\ (k\Omega) = V_{SETLOW}/I_{VREF}$$

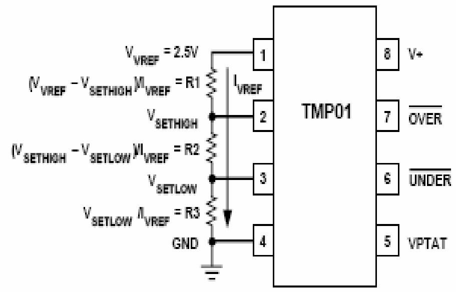

Figure 3. TMP01 Setpoint Programming

The total R1 + R2 + R3 is equal to the load resistance needed to draw the desired hysteresis current from the reference, or I_{VREF}.

The formulas shown above are also helpful in understanding the calculation of temperature setpoint voltages in circuits other than the standard two-temperature thermostat. If a setpoint function is not needed, the appropriate comparator should be disabled. SETHIGH can be disabled by tying it to V+, SETLOW by tying it to GND. Either output can be left unconnected.

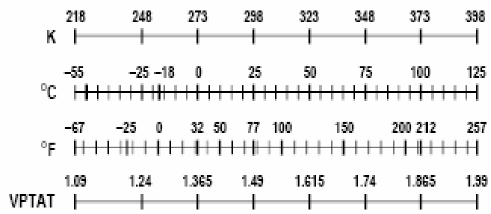

Figure 4. Temperature—VPTAT Scale

APPENDIX C

AD8009 AMPLIFIER DATA SHEET

In this appendix, selected pages of the data sheet of the AD8009 amplifier is given.

ANALOG DEVICES

1 GHz, 5,500 V/μs Low Distortion Amplifier

AD8009

FEATURES
Ultrahigh Speed
- 5,500 V/μs Slew Rate, 4 V Step, G = +2
- 545 ps Rise Time, 2 V Step, G = +2
- Large Signal Bandwidth
  - 440 MHz, G = +2
  - 320 MHz, G = +10
- Small Signal Bandwidth (–3 dB)
  - 1 GHz, G = +1
  - 700 MHz, G = +2
- Settling Time 10 ns to 0.1%, 2 V Step, G = +2

Low Distortion over Wide Bandwidth
- SFDR
  - –66 dBc @ 20 MHz, Second Harmonic
  - –75 dBc @ 20 MHz, Third Harmonic
- Third Order Intercept (3IP)
  - 26 dBm @ 70 MHz, G = +10

Good Video Specifications
- Gain Flatness 0.1 dB to 75 MHz
- 0.01% Differential Gain Error, R_L = 150 Ω
- 0.01° Differential Phase Error, R_L = 150 Ω

High Output Drive
- 175 mA Output Load Drive
- 10 dBm with –38 dBc SFDR @ 70 MHz, G = +10

Supply Operation
- +5 V to ±5 V Voltage Supply
- 14 mA (Typ) Supply Current

APPLICATIONS
- Pulse Amplifier
- IF/RF Gain Stage/Amplifiers
- High Resolution Video Graphics
- High Speed Instrumentations
- CCD Imaging Amplifier

FUNCTIONAL BLOCK DIAGRAMS

8-Lead Plastic SOIC (R-8)

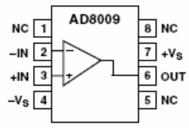

5-Lead SOT-23 (RT-5)

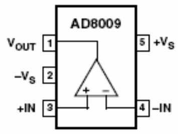

PRODUCT DESCRIPTION

The AD8009 is an ultrahigh speed current feedback amplifier with a phenomenal 5,500 V/μs slew rate that results in a rise time of 545 ps, making it ideal as a pulse amplifier.

The high slew rate reduces the effect of slew rate limiting and results in the large signal bandwidth of 440 MHz required for high resolution video graphic systems. Signal quality is maintained over a wide bandwidth with worst-case distortion of –40 dBc @ 250 MHz (G = +10, 1 V p-p). For applications with multitone signals, such as IF signal chains, the third order intercept (3IP) of 12 dBm is achieved at the same frequency. This distortion performance coupled with the current feedback architecture make the AD8009 a flexible component for a gain stage amplifier in IF/RF signal chains.

The AD8009 is capable of delivering over 175 mA of load current and will drive four back terminated video loads while maintaining low differential gain and phase error of 0.02% and 0.04°, respectively. The high drive capability is also reflected in the ability to deliver 10 dBm of output power @ 70 MHz with –38 dBc SFDR.

The AD8009 is available in a small SOIC package and will operate over the industrial temperature range –40°C to +85°C. The AD8009 is also available in an SOT-23-5 and will operate over the commercial temperature range of 0°C to 70°C.

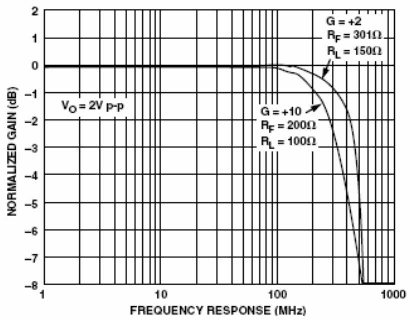

Figure 1. Large Signal Frequency Response; G = +2 and +10

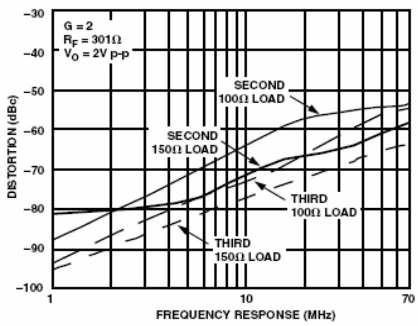

Figure 2. Distortion vs. Frequency; G = +2

REV. F

One Technology Way, P.O. Box 9106, Norwood, MA 02062-9106, U.S.A.
Tel: 781/329-4700 www.analog.com
Fax: 781/326-8703